Aspects of Molecular Medicine 5 (2025) 100077

Contents lists available at ScienceDirect

Aspects of Molecular Medicine

journal homepage: www.journals.elsevier.com/aspects-of-molecular-medicine

Potential antimicrobial properties of cytosine β-D-riboside derivatives through molecular dynamics and molecular docking exploration with bacterial and fungal proteins

Sarkar M.A. Kawsar [a,*], Rahnuma Tabassum [a], Nasrin Sultana Munia [a], Suraj N. Mali [b], Chin-Hung Lai [c], Jannatul Ferdous [a], Ferdausi Ali [d]

[a] Laboratory of Carbohydrate and Nucleoside Chemistry (LCNC), Department of Chemistry, Faculty of Science, University of Chittagong, Chittagong, 4331, Bangladesh
[b] School of Pharmacy, D. Y. Patil University (Deemed to Be University), Navi Mumbai, 400706, Maharashtra, India
[c] Department of Medical Applied Chemistry, Chung Shan Medical University, Taichung, 40241, Taiwan
[d] Department of Microbiology, Faculty of Biological Science, University of Chittagong, Chittagong, 4331, Bangladesh

ARTICLE INFO

Handling editor: A Angelo Azzi

Keywords:
Cytosine β-D-riboside
DMF/Et_3N
Antimicrobial
Molecular docking
MD

ABSTRACT

Nucleoside derivatives have contributed to the clinical and pharmaceutical fields as medicinal agents and approved drugs. The reaction of lauroyl chloride with cytosine β-D-riboside, i.e., cytidine (**1**) in DMF/Et_3N, was the initiator step leading to 5′-*O*-(lauroyl)cytidine (**2**). Compound (**2**) was reacted with various acylating agents and penetrated to give 2′,3′-di-*O*-acyl derivatives (**3**–**6**). Physicochemical, spectroscopical, and elemental analysis methods were used to confirm the structure of the synthesized derivatives. *In vitro* antimicrobial tests, coupled with PASS prediction, revealed that these derivatives are highly effective against distinct pathogenic bacteria. Compared with the standard nystatin, compound **5** exhibited excellent antifungal efficacy against *Aspergillus flavus* and *Aspergillus niger*. Molecular docking analysis was performed to evaluate the binding interactions with the FimH lectin domain from *E. coli* K12 and urate oxidase (Uox) from *Aspergillus flavus*. For the FimH lectin domain, the binding affinities range from −2.35 to −9.32 kcal/mol (PyRx) and from −0.764 to 115.318 kcal/mol (iGEMDOCK), where compound **2** exhibited the highest binding affinity and outperformed the standard azithromycin, forming hydrogen bonds with ASN A:138, GLN A:133, ASP A:54, ASN A:46, PHE A:1, and ASP A:47, along with Pi-alkyl interactions with TYR A:48. Similarly, compound **5**, among the other synthesized compounds, strongly bound to Uox, with docking scores of −8.65 kcal/mol (PyRx) and −119.145 kcal/mol (iGEMDOCK), interacting with key residues such as THR A:173, LEU A:170, PHE A:258, and HIS A:256 through van der Waals forces, Pi−Pi hydrophobic interactions, and hydrogen bonding. The RMSD, RMSF, and Rg analyses revealed that the docked complexes 4XO8:**2** and 1R4U:**5** exhibited stable protein−ligand interactions, with no significant structural deviations observed during the 100 ns MD simulations. The hydrogen bonding and SASA results further support the stability of these complexes. According to DFT and FMO studies, compound **5** should exhibit the highest chemical reactivity because it has the smallest Egap (4.84 eV). In silico, ADMET and toxicity studies were used to evaluate the pharmacokinetic characteristics, drug-likeness, and toxicity parameters of the newly synthesized compounds. Finally, SAR study was performed to predict any subsequent changes in the antimicrobial activities of these compounds modified at various positions in their structure, especially those modified with $[CH_3(CH_2)_{10}CO]$ and $\{CH_3(CH_2)_{14}CO\}$ groups. These results suggest that derivatives of lauroyl cytidine have great promise as antimicrobial agents for treating microbial infections.

1. Introduction

Antibiotic resistance has become a severe threat to public health, necessitating the discovery of novel and effective antimicrobial agents (Khan et al., 2024; Salam et al., 2023; Christaki et al., 2020; Ferri et al., 2017). The synthesis and consequent characterization of nucleoside analogs have been a vital area of research due to their extensive array of uses in medicinal and biological sciences (Wang et al., 2023; M.Z.H. Bulbul et al., 2021; Chowdhury et al., 2016). Cytidine, a nucleoside

* Corresponding author.
E-mail address: akawsarabe@yahoo.com (S.M.A. Kawsar).

https://doi.org/10.1016/j.amolm.2025.100077
Received 27 December 2024; Received in revised form 14 March 2025; Accepted 21 March 2025
Available online 24 March 2025

Abbreviations

ADMET	Absorption, distribution, metabolism, excretion, and toxicity
DFT	Density functional theory
FMO	Frontier molecular orbital
HOMO	Highest occupied molecular orbital
LUMO	Lowest unoccupied molecular orbital
MBC	minimum bactericidal concentration
MEP	Molecular electrostatic potential
MIC	minimum inhibitory concentration
PASS	Prediction of substance activity spectra
SAR	Structure–activity relationship

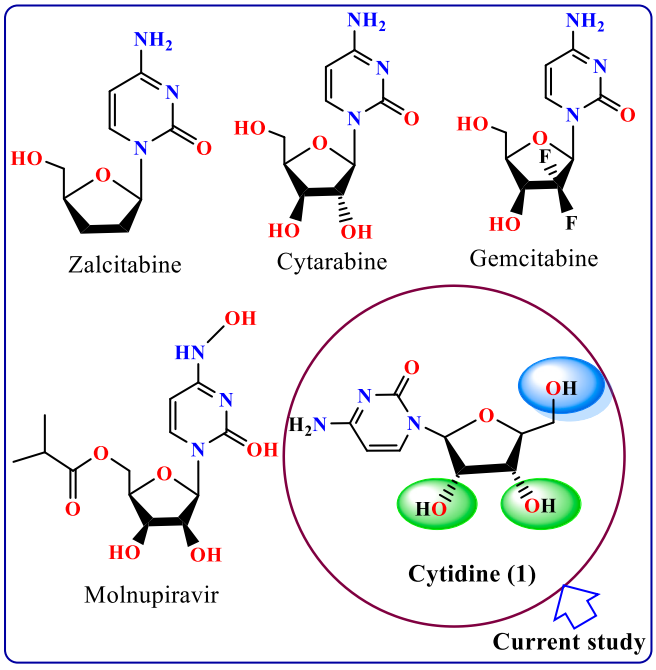

Fig. 1. Popular drugs that contain cytidine moieties in their structure are marketed.

comprising cytosine attached to a ribose sugar, serves as an excellent scaffold for drug development (Rohloff et al., 2015; Rana et al., 2020). Modifications at various positions on the cytidine molecule can increase its biological activity and improve its pharmacokinetic properties, potentially disrupting microbial DNA/RNA synthesis or other critical cellular processes (Bhuiyan et al., 2024; Sharma et al., 2014; Kawsar et al., 2021a, b). Examples of successful cytidine analogs include cytarabine, an analog of cytidine, which is used to treat leukemia and lymphoma among different cancers. It disrupts DNA synthesis, which is integrated into the DNA of cancer cells and ultimately leads to cell death (Löwenberg et al., 2011; Di Francia et al., 2021). Gemcitabine is a drug used to treat cancer, whereas zalcitabine is an antiretroviral medication for HIV/AIDS (Toschi et al., 2015; Adkins et al., 1997). The TVV inhibitory agents 2′-C-methylcytidine (2CMC) and 7-Deaza-2′-C-methyladenosine (7d2CMA) are derived from the migration of two acidic protons of the N-4-hydroxylcytosine fragment of a drug called Molnupiravir, which shows promise as an effective treatment for COVID-19 (Pourkarim et al., 2022; Narayanasamy et al., 2022). Certain types of cancer are treated with other cytidine derivatives, such as decitabine and azacytidine, which function as epigenetic modulators by altering the expression of genes in malignant cells (Stresemann and Lyko, 2008; Vogler et al., 1976). Some popular marketed drugs containing cytidine moieties are shown in Fig. 1. Considering the attributes above and in pursuit of discovering innovative therapeutics, we have made notable progress in our current investigation. Various acylating agents have been introduced into the 2′, 3′, and 5′ positions of cytidine to synthesize unprecedented cytidine derivatives via the regioselective direct acylation method (Kawsar and Ferdous, 2021a). Upon synthesis, these derivatives undergo rigorous evaluation to assess their efficacy against a spectrum of bacterial and fungal pathogens. Experimental assays, including minimum inhibitory concentration (MIC), minimal bactericidal concentration (MBC) determination, and zone of inhibition studies, provide valuable insights into the compound's potency and spectrum of activity (A.U. Islam et al., 2024). Structure–activity relationship (SAR) studies further elucidate the relationship between biological activity and chemical structure, guiding the design of more potent derivatives (M.M. Islam et al., 2024; Sultana et al., 2024). In parallel, computational methods play a pivotal role in characterizing cytidine derivatives at the molecular level. Density functional theory (DFT) and frontal molecular orbital (FMO) calculations offer insights into the electronic structure, reactivity, and stability of compounds (Jayavel et al., 2024a; Z.H. Bulbul et al., 2021). Furthermore, molecular electrostatic potential (MEP) calculations shed light on the distribution of electron density on the surface of cytidine derivatives, which is correlated with their interactions with biological targets and influences their pharmacological activity (Kawsar et al., 2024a; Akter et al., 2024; Murray and Politzer, 2011). Additionally, PASS uses computational algorithms to predict the biological activity profile of compounds on the basis of their chemical structure, aiding in identifying potential antimicrobial agents (Nepolraj et al., 2021; Shamsuddin et al., 2021; Islam et al., 2022). ADMET properties are crucial in the development of new drugs, including cytidine derivatives.

Understanding these pharmacokinetic properties helps predict a drug's behavior in the body and ensures its efficacy and safety (Sampathkumar et al., 2024; Kawsar et al., 2022a; Hosen et al., 2023). Key factors include gastrointestinal (GI) absorption, blood–brain barrier (BBB) penetration, cytochrome P450 interactions, and the partition coefficient (log P) (Rana et al., 2021). In addition to Lipinski's rule of five, the Ghose, Veber, and Egan rules provide a framework for optimizing these compounds (Lipinski et al., 2012). Lipinski's rules focus on the molecular properties affecting oral bioavailability (Jayavel et al., 2024b). Moreover, Ghose, Veber, and Egan offer additional guidelines for molecular weight, solubility, and polar surface area, enhancing the drug development process of cytidine derivatives (Najar et al., 2020). Molecular docking simulations further elucidate the molecular interactions between cytidine derivatives and their target biomolecules, such as enzymes or receptors involved in microbial growth or virulence. These simulations predict the binding mode and affinity of the compounds, guiding the rational design of novel antimicrobial agents with enhanced efficacy and selectivity (Kawsar et al., 2022b). Moreover, molecular dynamics simulations provide dynamic insights into the behavior of cytidine derivatives over time, revealing conformational changes, interactions with solvent molecules, and stability in biological environments (Tabassum et al., 2024; Arzine et al., 2024). FimH is a well-characterized lectin that bacteria use to adhere to glycosylated surfaces, including cells (Tiralongo and Moran, 2010). Cell–cell adhesion often involves catch–bonds, which increase the lifetime of adhesin–receptor complexes under mechanical stress. These bonds are crucial in leukocyte recruitment, tissue integrity, and bacterial infections. They are also vital in bacterial infections, such as those caused by uropathogenic *E. coli*, leading to urinary tract infections (UTIs) (Imberty, 2011). A key step in *E. coli* infection is adhesion to urothelial cells, which is mediated by type 1 pili—proteinaceous filaments on the bacterial surface. Type 1 pili consist of up to 3000 FimA subunits and other components, such as FimF, FimG, and FimH. FimH, located at the pilus tip, binds specifically to terminal α-D-linked mannoses on

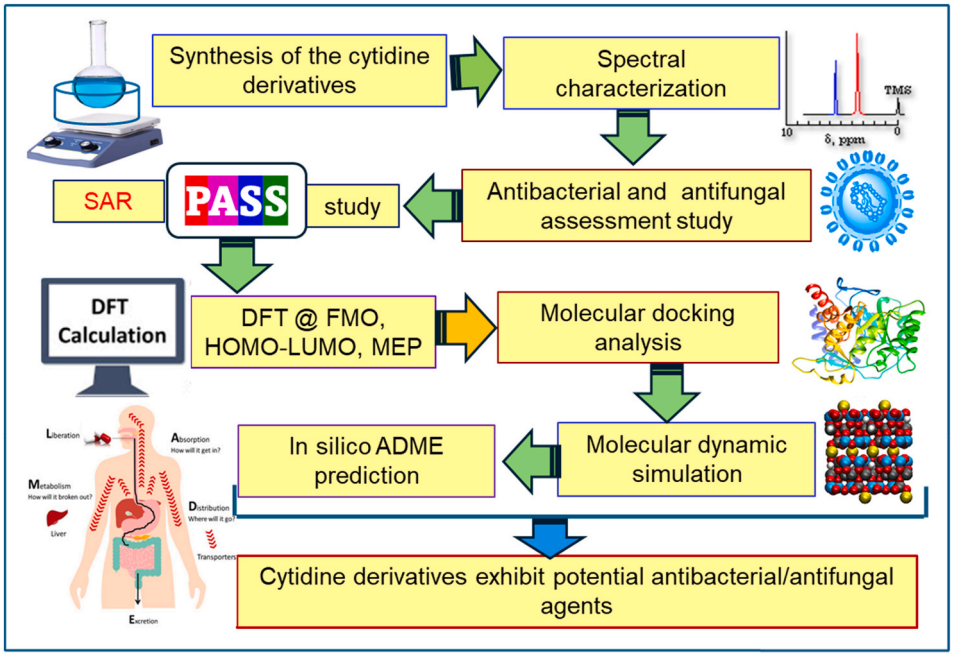

Fig. 2. Schematic flow chart of the current study.

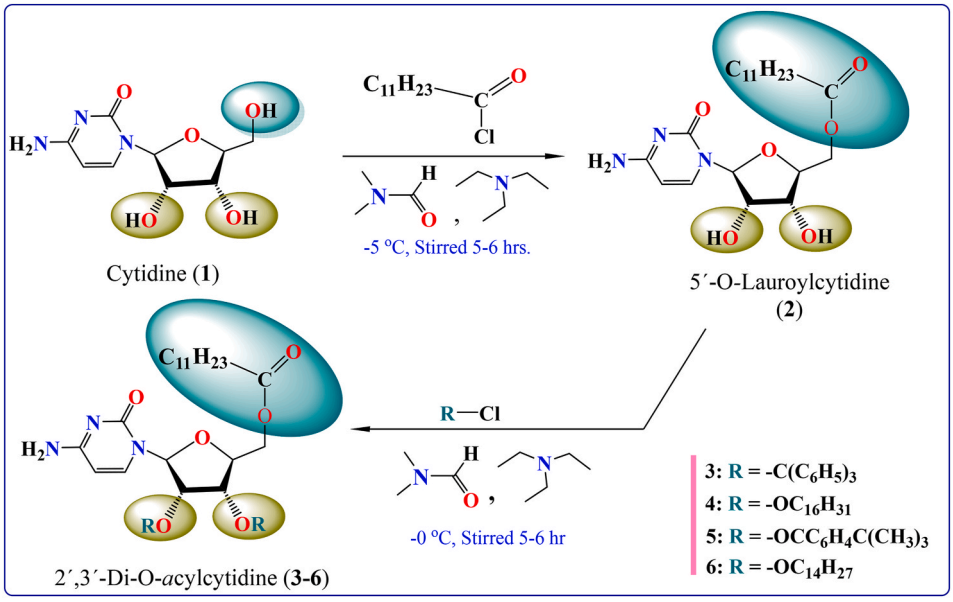

Scheme 1. Synthetic pathway and acylating agents used for accessing cytidine derivatives **2**–**6**.

uroplakin 1a of urinary epithelial cells via catch–bond interactions. Owing to its role in infection, FimH is a target for antiadhesive drug development. The structure of FimH includes an N-terminal mannoside-binding domain (FimHL) and a C-terminal pilin domain (FimHP), whose interaction is essential for catch-bond formation (Bouckaert et al., 2005). Numerous natural and synthetic mannosidic ligands for FimH have been developed and tested for their ability to inhibit this binding. However, glycans, particularly carbohydrates, have been linked to cancer, inflammation, and bacterial infections. Different lectin–glycan interactions have improved immunotherapies, antivirals, and vaccines (Matsumoto et al., 2012; Fujii et al., 2011).

This integrated approach aims to develop novel cytidine derivatives with potent antimicrobial activity and favorable pharmacokinetic profiles, addressing the urgent need for new antimicrobial agents. In this work, we successfully synthesized and characterized a series of cytidine derivatives, demonstrating their potential as effective antimicrobial agents. The combination of experimental and computational data provides a comprehensive understanding of their properties. Some derivatives have emerged as the most promising candidates, showing significant antibacterial and antifungal activities, favorable ADMET properties, and robust interactions with target proteins. Future research will focus on further optimization of these derivatives and exploration of their clinical applications. Fig. 2 shows a flow diagram of the work plan.

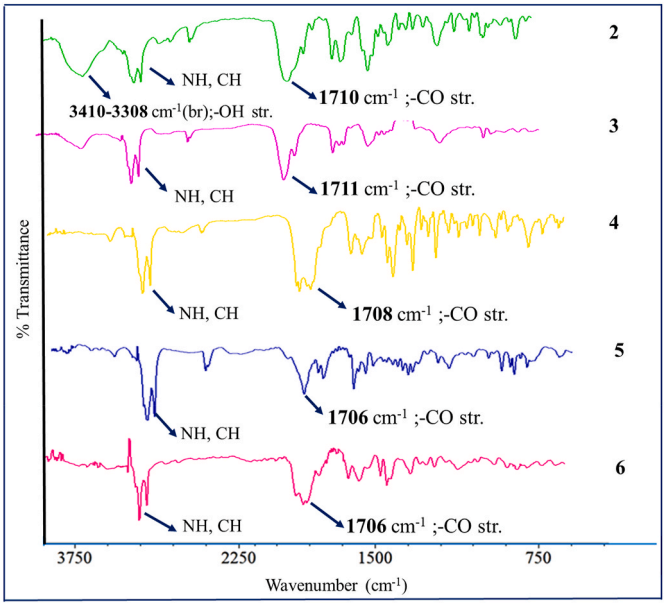

Fig. 3. FTIR spectra of compounds **2–6**.

Table 1
The zone of inhibition was observed against gram-positive and gram-negative bacteria by derivatives **1**–**6**.

Diameter of inhibition zones (in mm)					
Entry	*B. cereus* (G + ve)	*B. subtilis* (G + ve)	*S. typhi* (G -ve)	*E. coli* (G -ve)	*P. aeruginosa* (G -ve)
1	NI	NI	NI	NI	NI
2	12.75 ± 1.0	11.20 ± 1.1	13.25 ± 1.0	13.00 ± 0.5	10.25 ± 1.0
3	NI	NI	NI	NI	NI
4	8.50 ± 0.5	8.00 ± 0.5	10.50 ± 1.1	NI	12.50 ± 0.5
5	NI	NI	13.50 ± 0.5	NI	14.75 ± 0.5
6	NI	NI	NI	8.00 ± 1.1	NI
Azithromycin	17.75 ± 1.0	18.00 ± 0.5	18.00 ± 1.0	18.00 ± 1.1	18.50 ± 1.1

The data are presented as the means ± SDs, and the values are representative of triplicate experiments. Statistically significant inhibition ($p < 0.05$) is marked with an asterisk (*) for the test compounds and a double asterisk (**) for the reference antibiotic azithromycin. NI = no inhibition.

2. Materials and methods

2.1. Materials and equipment

Analytical-grade solvents were utilized and purified via standard procedures. All reagents were commercially available from Sigma–Aldrich (Germany) and were used as received unless otherwise specified. The melting points of the compounds were determined via an electrothermal melting point apparatus (Fisher Scientific, Hampton, NH, USA). The reported values are uncorrected for solid and thoroughly dried compounds. A vacuum rotary evaporator was used to evaporate the solvent under reduced pressure (BUCHI, Flawil, Switzerland). TLC separations were performed on a Kieselgel GF_{254} column (Germany), and column chromatography was carried out using silica gel G_{60}. Infrared spectra were recorded via an FTIR spectrophotometer (IR Prestige-21, Shimadzu, Japan) at the Department of Chemistry, University of Chittagong. ^{1}H and ^{13}N NMR spectra were recorded via a Brucker 400 MHz spectrometer at WMSRC, JU, Bangladesh.

2.2. Synthesis

2.2.1. 5′-O-(Lauroyl)cytidine (2)

Cytidine (**1**) (74 mg, 0.307 mmol) in anhydrous dimethyl formamide (DMF) (3 mL) and triethylamine (0.15 mL) were chilled to 0 °C, after which lauroyl chloride (0.0724 mL, 1.1 molar equivalents) and a catalytic amount of 4-dimethylaminopyridine (DMAP) were introduced into a round-bottom flask. After 6 h at 0 °C, the reaction mixture was allowed to sit all through the night at ambient temperature with continuous stirring. The complete conversion of the initial material into a rapidly migrating single product was identified *via* TLC (methanol-chloroform, 1:24). Standard work-up procedures and purification via column chromatography with methanol-chloroform (1:24 as the mobile phase) generated the lauroyl derivative (**2**) (106.6 mg) as a crystalline solid.

Yield = 82.36 %, m.p. = 44–45 °C, EtOAC-*n*-C_6H_{14}. *Rf* = 0.50, CH_3OH–$CHCl_3$ (1:24 as the mobile phase).

The spectral data are presented in the Supplementary data file in 1.

2.2.2. General procedure for the synthesis of lauroyl derivatives 3-6

A cooled (0 °C) and stirred solution of lauroyl derivative **2** (56.6 mg, 0.133 mmol) in DMF (3 mL) and triethylamine (0.15 mL) trityl chloride (0.1439 g, 4 M eq.) was added. After 6 h of swirling at 0 °C, the resulting mixture was stirred at room temperature overnight. TLC analysis (methanol-chloroform, 1:24) demonstrated the complete conversion of the reactant into a single product. Upon passing the final product through a silica gel column containing methanol-chloroform (1:24) as the eluent, the lauroyl derivative **3** (120 mg) was obtained as a solid. Similarly, compounds **4** (102.70 mg) as needles (palmitoyl derivatives), **5** (66 mg) as needles (4-*t*-butylbenzoyl derivatives), and **6** (62.20 mg) as needles (myristoyl derivatives) were produced *via* identical purification and reaction techniques.

2.2.3. 5′-O-Lauroyl-2′,3′-di-O-(trityl)cytidine (3)

Yield = 98.97 %, m.p. = 153–154 °C, EtOAC-*n*-C_6H_{14}. *Rf* = 0.52, CH_3OH–$CHCl_3$ (1:26).

The spectral data are presented in the supplementary data file.

2.2.4. 5′-O-Lauroyl-2′,3′-di-O-(palmitoyl)cytidine (4)

Yield = 72.58 %, m.p. = 57–58 °C, EtOAC-*n*-C_6H_{14}. *Rf* = 0.55, CH_3OH–$CHCl_3$ (1:25).

The spectral data are presented in the supplementary data file.

2.2.4.1. 2′,3′-Di-O-(4-t-butylbenzoyl)-5′-O-(lauroyl)cytidine (5)

Yield = 78.46 %, m.p. = (145–150) °C, EtOAC-*n*-C_6H_{14}. *Rf* = 0.53, CH_3OH–$CHCl_3$ (1:24).

The spectral data are presented in the supplementary data file.

2.2.4.2. 5′-O-Lauroyl-2′,3′-di-O-(myristoyl)cytidine (6)

Yield = 92.84 %, m.p. = 70–71 °C, EtOAC-*n*-C_6H_{14}. *Rf* = 0.51, CH_3OH–$CHCl_3$ (1:26).

The spectral data are presented in the supplementary data file.

2.3. In vitro antimicrobial activity test

2.3.1. Tested microorganisms

In the examination of antimicrobial activity conducted in vitro, a total of seven different types of microorganisms were utilized. These included two types of gram-positive bacteria, *Bacillus subtilis* (ATCC 6633) and *Bacillus cereus* (BTCC 19); three types of gram-negative bacteria, *Escherichia coli* (ATCC 8739), *Salmonella typhi* (AE 14612), and *Pseudomonas aeruginosa* (ATCC 9027); and two types of fungi, *Aspergillus niger* (ATCC 16404) and *Aspergillus flavus* (ATCC 204304). These microbial strains were sourced from the Microbial Laboratory located in

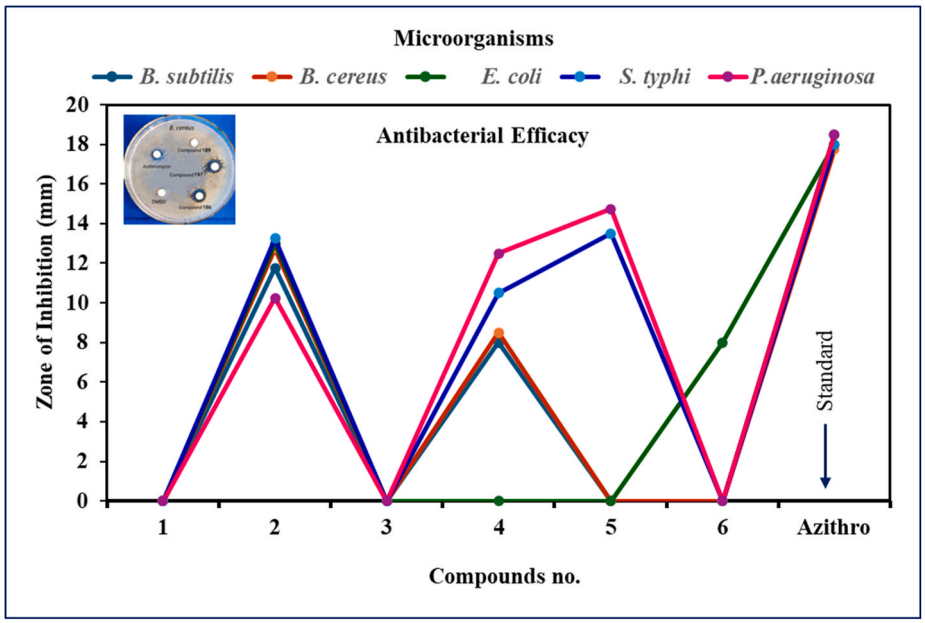

Fig. 4. Zone of inhibition (mm) observed against five human pathogenic microorganisms.

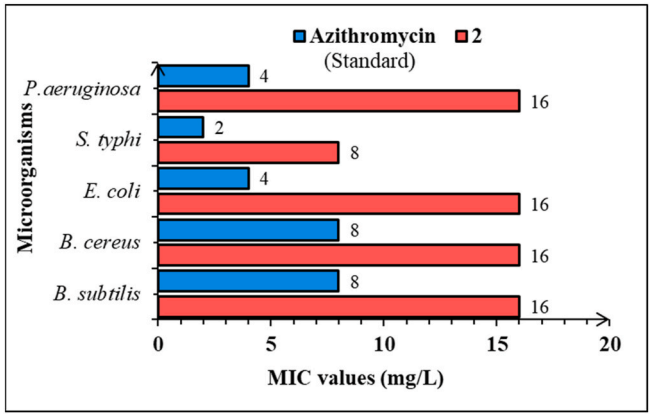

Fig. 5. MIC values of compound **2** against the tested species.

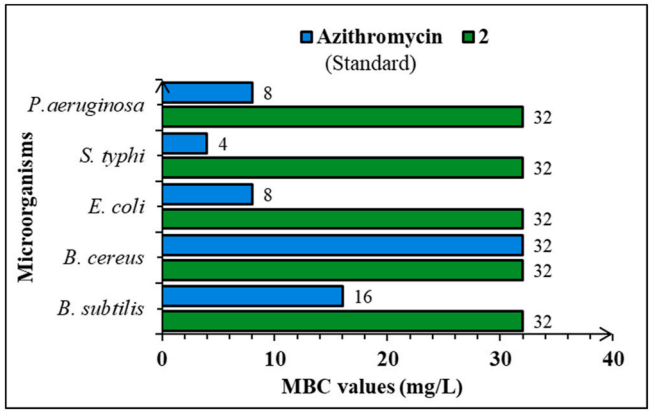

Fig. 6. MBC values of **2** against the tested species.

the Department of Microbiology at the University of Chittagong, Bangladesh.

Table 2
Percentage inhibition of fungal growth by synthesized compounds against fungal organisms.

% inhibition of fungal growth in mm (20 μg/μL)		
Compound	*Aspergillus flavus*	*Aspergillus niger*
1	NI	NI
2	25.31 ± 1.0	42.25 ± 1.1
3	NI	NI
4	33.92 ± 1.0	53.67 ± 1.0
5	**69.07 ± 1.1	**78.28 ± 1.0
6	NI	NI
Nystatin	63.40 ± 1.0	64.55 ± 1.0

The data are presented as the means ± SDs, and the values are representative of triplicate experiments. Statistically significant inhibition ($p < 0.05$) is marked with an asterisk (*) for test compounds and a double asterisk (**) for the reference Nystatin. NI = no inhibition.

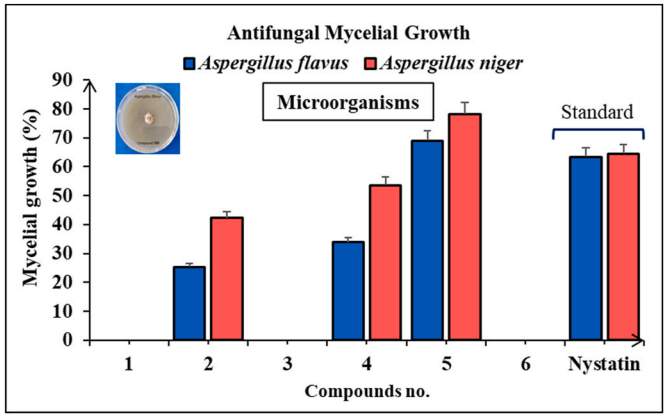

Fig. 7. Percent inhibition of the two fungal strains by synthesized derivatives.

2.3.2. Antibacterial assessments

The synthesized derived products were subjected to antibacterial inspections via the conventional disk diffusion procedure following the guidelines outlined by the CLSI (Bauer et al., 1966; CLSI, 2018). The test

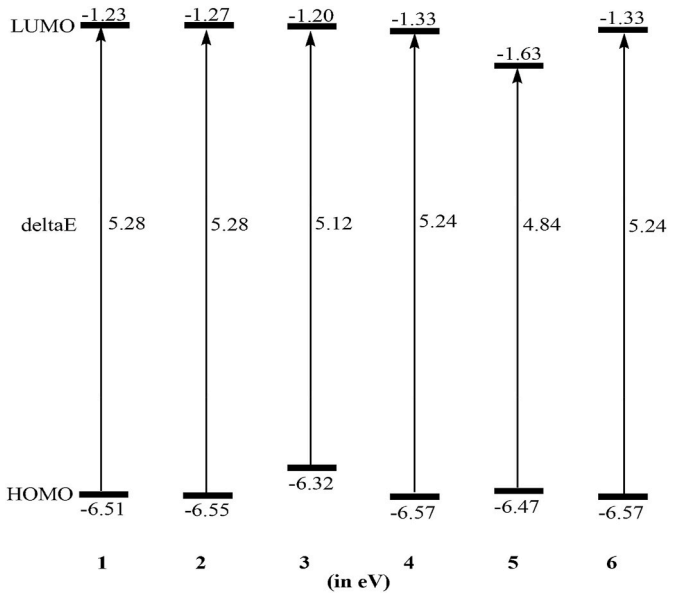

Fig. 8. ΔEs of the cytidine derivatives studied (in eV).

bacteria were suspended in sterilized saline water (0.9 %) acquired from dishes via a sterile inoculating loop to prepare the inoculum. The density of the suspension was calibrated by juxtaposing it with the McFarland 0.5 standard. Afterward, all bacteria were dispersed onto Petri dishes with Mueller–Hinton agar. A total of 10 μL of each test substance was carefully dispensed onto 6 mm filter paper discs (Hi-Media) via an Eppendorf pipette, which was subsequently placed onto the agar medium. Petri dishes inoculated with harmful bacteria were then nurtured in an incubator at 36 °C for one day to encourage the proliferation of the microorganisms. The outcomes were evaluated by gauging the diameter of the inhibitory regions on a millimeter scale. Azithromycin-containing discs (Square Pharmaceuticals PLC, Bangladesh) served as the reference antibiotic and positive control and were assessed under the same conditions as the test substances.

2.3.3. MIC and MBC determination

The microdilution method was used to elucidate the minimum inhibitory concentration (MIC) and minimum bactericidal concentration (MBC) (Balouiri et al., 2016). The synthesized compounds were subjected to serial twofold dilutions, ranging from 8.0 to 0.25 mg/mL, in Mueller–Hinton broth supplemented with five percent dimethyl sulfoxide (DMSO). Our initial investigations confirmed that five percent DMSO did not impact bacterial growth. A calibrated microbial suspension of 5 μL was added to each well, which contained 100 μL of the diluted substance. All the wells were then filled with 95 μL of sterile Luria–Bertani broth. A negative control containing all the components, excluding the bacterial mixture, was added. After a 12-h incubation at 35 °C, 20 mL of 2 mg/mL p-iodonitrotetrazolium chloride was added to each microplate. A purple–red tint emerged after 30 more minutes of incubation, indicating the proliferation of bacteria and the conversion of INT to formazan. We pinpointed the minimum compound concentration needed to halt bacterial growth after a 24-h exposure period for MIC determination. To investigate the MBC, we transferred the diluted samples from the MIC trial onto unseeded Luria–Bertani agar plates and then allowed them to incubate for 18–24 h. The MBC was identified as the maximum dilution where zero distinct microbial colonies were visible.

2.3.4. Mycelial growth assessment

The “mycelial proliferation test” with the “food poisoned” strategy was used to assess the efficacy of the compounds that were produced against the development of fungi (Hantosh et al., 2015; Hosen et al., 2022). The experiment was conducted using standard potato dextrose agar (PDA) media as the substrate. Using a sterilized pipette, 0.1 mL (or 1 mg) of each test substance that had been solubilized in dimethyl sulfoxide to reach a dosage of 1 % (w/v) was added to a sterile Petri plate. The Petri dish was subsequently filled with 20 mL of medium, mixed well, and left to set. A block of spores (5 mm) taken from each fungus was placed in the middle of each Petri dish to complete the inoculation process. These blocks of spores were retrieved with a cork borer from the frequently rising section of 7-day-old fungal colonies on potato dextrose agar. Following inoculation, the Petri dishes were cultivated in an incubator at 25 ± 2 °C. Three replications of this assessment approach were conducted, utilizing appropriate control plates containing potato dextrose agar without any test chemicals. After five days of incubation, the diameter of each fungus’s circumferential mycelial development was measured in millimeters. The following equation was used to determine the percentage of mycelial growth inhibition by the test fungus:

$$I = (C - T)/C \times 100$$

In this context, “I" signifies the percentage of inhibition, “C" indicates the diameter of the fungal colony in the control solution (DMSO), and “T" represents the diameter of the fungal colony in the treatment group.

2.4. Structure–activity relationship (SAR)

SAR studies are important for understanding the relationship between the molecular composition and biological action of cytidine derivatives. The key functional groups and structural features responsible for the observed biological effects can be identified by systematically modifying the molecular structure and evaluating the corresponding antimicrobial activity. This information can guide the rational design of more potent derivatives. Hunt and Kim’s concepts of membrane permeation are utilized in pharmaceutical design via this well-known methodology (Hunt, 1975; Kim mi et al., 2007).

2.5. DFT-based compound optimization

DFT optimization of the gas-phase configurations of the examined compounds (Figs. 8 and 9) was conducted via the 6-311++G** basis set (McLean and Chandler, 1980; Krishnan et al., 1980). The DFT computation utilized the hybrid B3LYP approach, which, following Becke’s concept, incorporates a blend of exact (HF) and DFT exchange via the B3 functional, along with the LYP correlation functional (Becke, 1993; Lee et al., 1988). Provided that computational resources permit, harmonic vibrational frequencies are computed at a similar theoretical stage to verify that the quantity of hypothetical frequencies is nil at the stationary point after the geometry of the individual molecule converges (Miehlich et al., 1989). Gaussian 09 software was used to calculate the harmonic vibrational frequency and optimize the shape of the compounds (Frisch, 2013).

2.6. Frontier molecular orbital (FMO) analysis

FMO theory was employed with the aid of B3LYP/6-311++G(d,p) basis sets to scrutinize the electrical and optical properties of these synthesized molecules. These molecules were determined to be neutral and of singlet multiplicity. FMO theory validates frontier molecular orbitals, which are the highest occupied molecular orbital (HOMO) and lowest unoccupied molecular orbital (LUMO). The HOMO, because it is the outermost electron-containing orbital, becomes a donating site of electrons, and conversely, when an orbital’s population is sparse and thus devoid of energy-carrying capacity, such as having extra available slots for further additional valence shells, one can decide that this will be classed simply as LUMOs or, upon conditionally stating, become

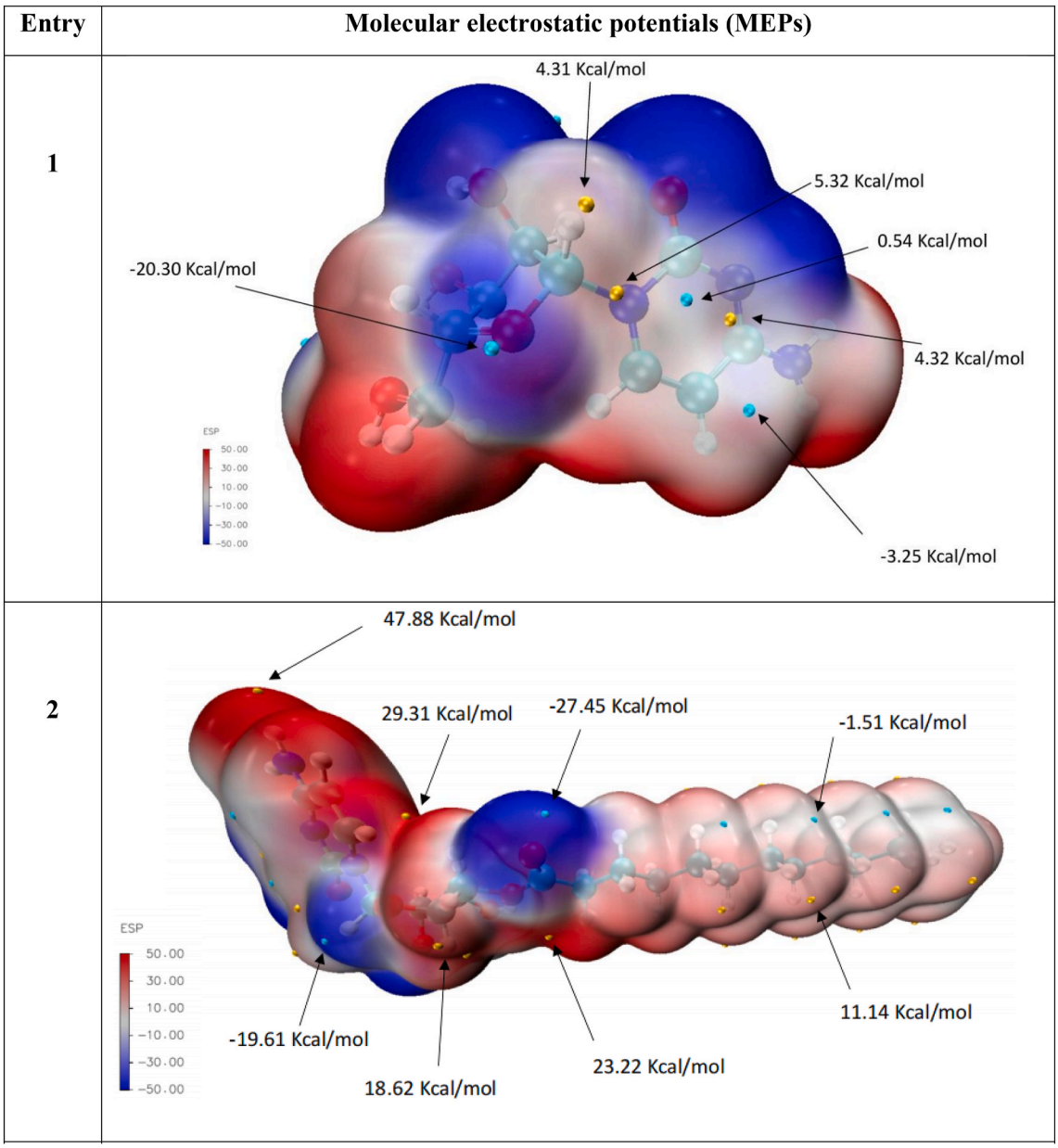

Fig. 9. MEPs of the studied compounds (the default setting of Multiwfn).

acceptive toward incoming chronic disturbances. The number of donor electrons of a molecule is correlated with its HOMO energy (E_{HOMO}), and a higher E_{HOMO} value indicates a greater electron-donating tendency (Becke, 1998). Numerous metrics, including softness, electronegativity, chemical hardness, the electrophilicity index, and the energy gap (ΔE) between the HOMO and LUMO, were calculated. Gaussian09 was used to conduct the FMO analysis, and GaussView 6.1.1 was used to present the outcomes (Dennington et al., 2016).

Electrophilicity index : $\omega = \mu^2/(2\eta)$

electronegativity : $\mu = -(I+A)/2$

chemical hardness : $\eta = (I-A)/2$

Softness : $S = 1/(2\eta)$

where I and A are the ionization energy and electron affinity of the species, respectively.

Moreover, Koopmans' theory ($I = -E_{HOMO}$ and $A = -E_{LUMO}$) can be used to compute a species's ionization energy (I) and electron affinity (A) (Koopmans, 1934).

2.7. Molecular electrostatic potential (MEP)

This study aimed to examine the orientation and spatial configuration of functional groups in chemical structures (Suresh et al., 2022). The MEPs of the synthesized compounds were investigated via computational methods. Molecular structures were constructed and optimized with Gaussian 09, employing the B3LYP/6-311++G(d,p) level of theory to achieve accurate geometric configurations. The MEP was then calculated via the generated.fchk file and the Multiwfn program (Lu and Chen, 2012; Lu and Feiwu Chen, 2012), which provided insights into the electrostatic interactions of the molecules. The MEP surfaces were color-coded to highlight areas of different electrostatic potentials. In this

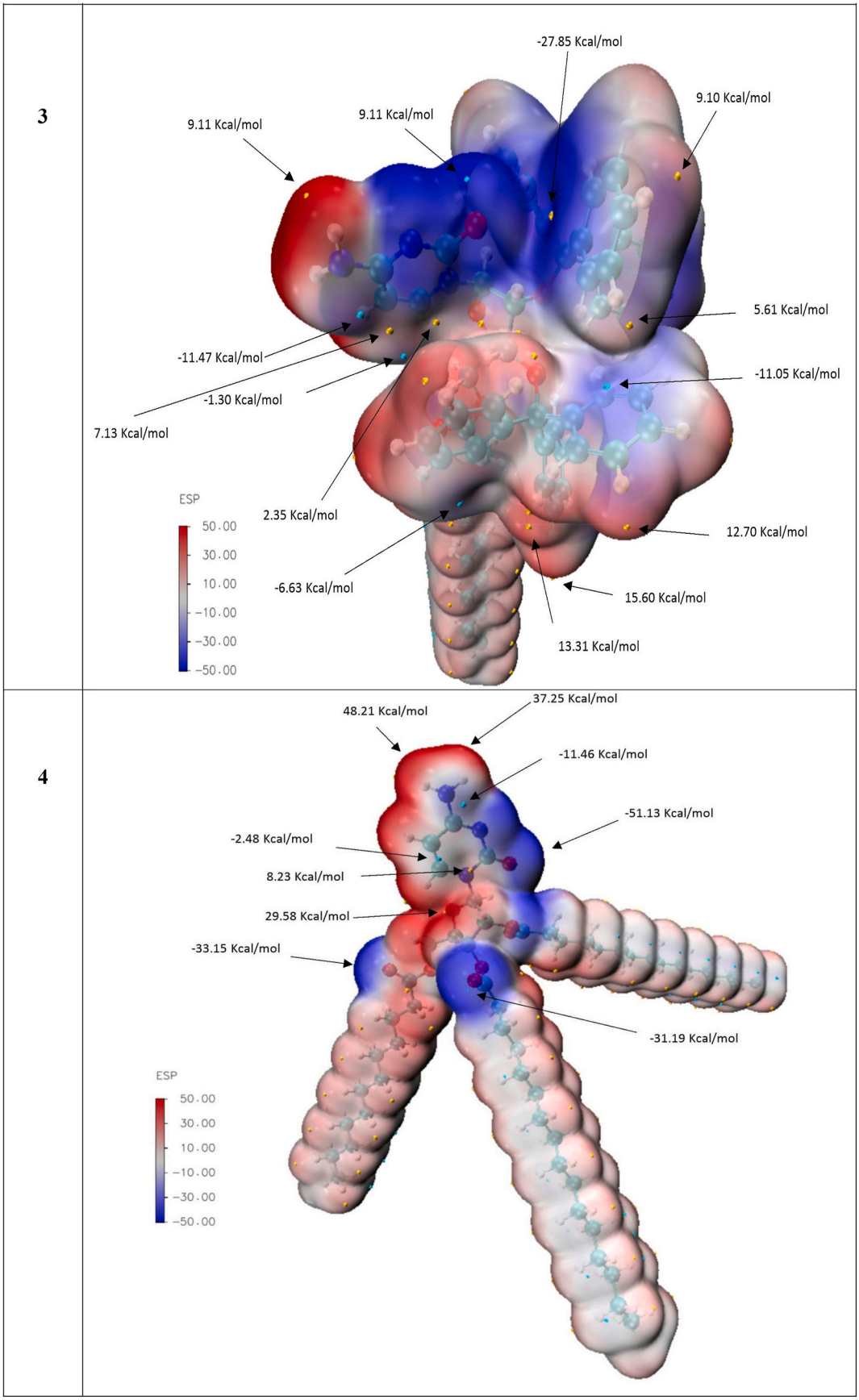

Fig. 9. (*continued*).

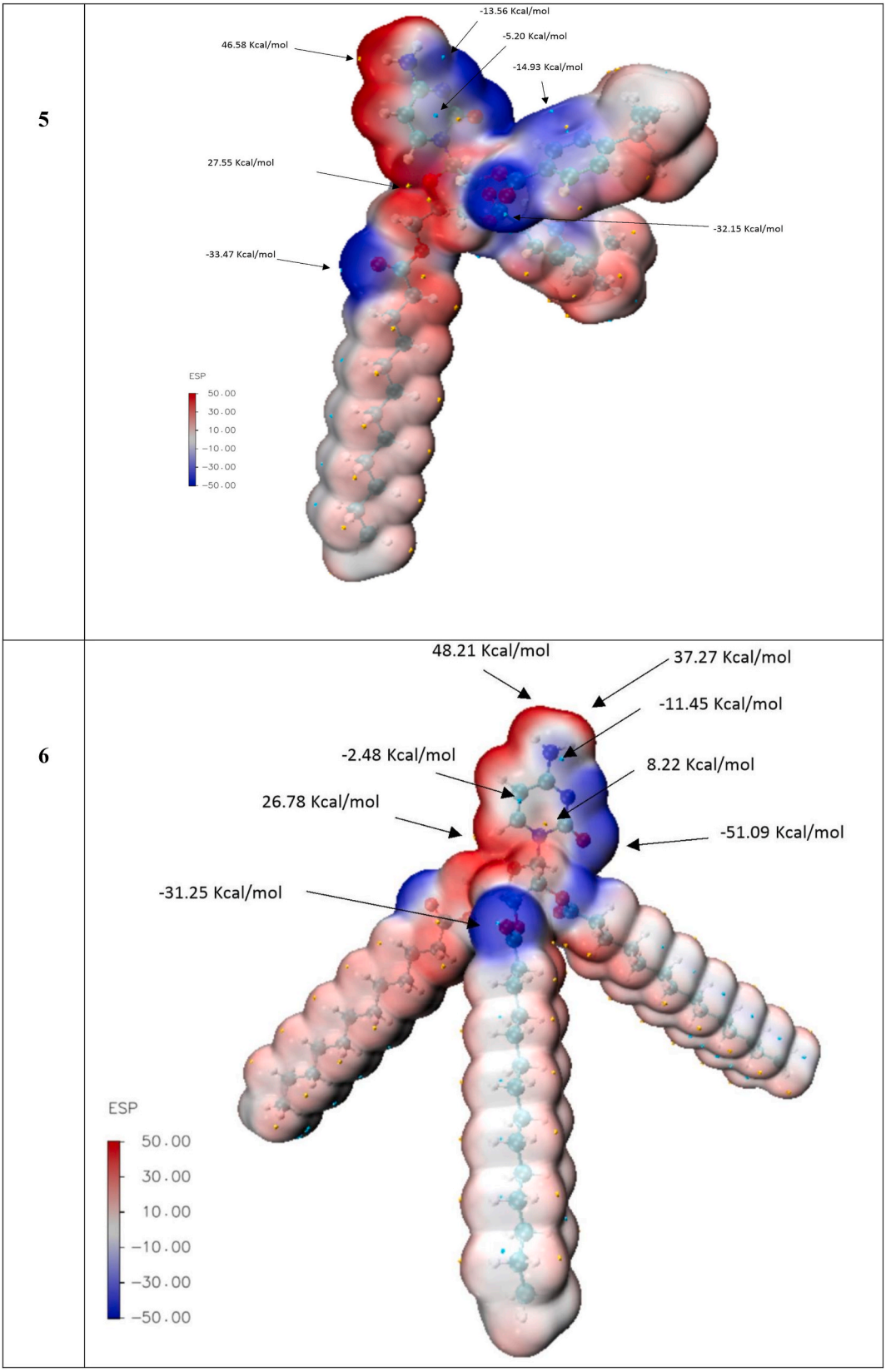

Fig. 9. (*continued*).

study, positive potential regions are depicted in red, indicating electrophilic areas, whereas negative potential regions are shown in blue, reflecting nucleophilic areas. Intermediate potentials are represented in varying shades of green and yellow. The visual representations helped identify key regions of the molecules where electrostatic interactions might be strongest, such as potential binding sites (Murray and Politzer, 2011).

Table 3
Energy of the highest-occupied molecular orbital (E_{HOMO}), energy of the lowest-unoccupied molecular orbital (E_{LUMO}), dipole moment (D), and quantum chemical descriptors.

	E_{HOMO} (eV)	E_{LUMO} (eV)	D (Debye)	μ (eV)	η (eV)	S (eV^{-1})	ω (eV)
1	−6.5133	−1.2338	9.2900	3.8736	2.6398	0.3788	2.8420
2	−6.5536	−1.2659	7.3397	3.9097	2.6438	0.3782	2.8909
3	−6.3248	−1.2017	4.4134	3.7633	2.5616	0.3904	2.7643
4	−6.5715	−1.3293	3.1943	3.9504	2.6211	0.3815	2.9769
5	−6.4722	−1.6328	3.5655	4.0525	2.4197	0.4133	3.3926
6	−6.5718	−1.3284	3.1896	3.9501	2.6217	0.3814	2.9759

2.8. PASS predictions

The PASS web application (Lagunin et al., 2000) (http://www.pharmaexpert.ru/passonline/) was used to predict the antimicrobial activity of compounds **1–6**. The compounds' structures were first converted to 'SMILES' formats via SwissADME (http://www.swissadme.ch). The PASS provides activity predictions through the probability of activity (Pa) and probability of inactivity (Pi) scores, which range from 0.00 to 1.00. These scores do not always sum to 1.00, as predictions are made independently.

2.9. Pharmacokinetic properties and toxicity

To prevent drug failure in the clinic, the ADMET (absorption, distribution, metabolism, excretion, and toxicity) properties of compounds **1–6** were evaluated via an in silico tool (Pires et al., 2015). We assessed their absorption in the human intestine, blood−brain barrier permeability, metabolism, clearance, and toxicity. Drug likeness was evaluated via Lipinski's rule of five (molecular weight <500 Da, ≤5 hydrogen-bond donors, ≤10 hydrogen-bond acceptors, and logP ≤5), with properties obtained from the 'SwissADME' server (www.swissadme.ch) (Mali and Pandey, 2021) and toxicity analysis by Osiris (Pires et al., 2015). Additional drug likeness was assessed via rule-based filters from the Lipinski, Ghose, Veber, and Egan rules.

2.10. Molecular docking analysis

To determine how synthesized compounds bind to enzyme active sites, we employed molecular docking with the 'FimH' lectin domain from *E. coli* K12 (PDB ID: 4XO8) and urate oxidase from *Aspergillus flavus*. For this purpose, 2D structures were first obtained via ChemDraw *v.* 15.0, converted to 3D forms, and optimized via the MM2 force field in ChemBio3D *v.* 12.0 (Gurav et al., 2024). The 3D crystal structures of the enzymes were sourced from the Protein Data Bank (PDB ID: 1R4U, Resolution: 1.65 Å). The receptor structures were refined with Swiss PDB Viewer *v* 4.1.0, which included water removal and the addition of hydrogen atoms for accurate ionization and tautomeric states. The docking simulations were carried out via the docking suite PyRx (embedded with AutoDock and Vina). The docking score obtained by PyRx was also checked with scores obtained from iGemDock V. 2.1. For PyRx (Kondapuram et al., 2021), the universal force field (UFF) with conjugate gradient settings was used for docking, with a search space centered at (40, 40, 50) Å and dimensions of (80, 80, 80) Å. Simulations were run with an exhaustiveness setting of 8 to find the lowest energy pose. The docking approach was validated by redocking the crystallized ligand SAC into the binding pocket of 1R4U and comparing the poses to those of the crystallized structure and 2D interaction diagram obtained by Ligplus (Rana et al., 2021).

2.11. Molecular dynamics simulations

To assess the structural stability of the complexes and their residue and atom behavior, we carried out molecular dynamics (MDS) simulation analysis via the popular software GROMACS 5.1.2 with GROMACS 96−53a6 force fields (Kondapuram et al., 2021). All the topology files for the ligands were generated via the Dundee PRODRG 3.0 server. The best docked compounds, 4XO8:**2** and 1R4U:**5**, were simulated along with their protein complexes for a period of 100 ns. These MDS models were solvated via an explicit simple point charge (SPC) water model, and the box type used was triclinic. These systems were neutralized with charged ions to replace the SPC water molecules. The energy minimization parameter is used with the steepest descent for up to 5000 steps. After that, NPT equilibrium was maintained as per the standard formats (temperature (K) = 300; pressure = 1 bar; and simulation time = 100 ns). For both of these simulations, visualizations were performed with the GROMACS package (Mali and Pandey, 20221).

2.12. Statistical analysis

The experimental outcomes are presented as the means ± standard errors for each parameter investigated, based on three replicates. The t tests were used for statistical analysis, and a p value threshold of not more than 0.05 was deemed statistically significant. Additionally, all the data were verified for a normal distribution and homogeneity of variance before the t tests were conducted to ensure the validity of the results.

3. Results and discussion

3.1. Synthetic characterization

The main objective of this research was to synthesize a series of cytidine derivatives containing a wide variety of substituents in a single-molecule framework to assess their biological activities. Fig. 2 displays a thorough diagram outlining the research workflow, highlighting the successive stages, strategies, and significant components. In Scheme 1, the synthesis process began with the preparation of 5′-*O*-lauroylcytidine (**2**) by reacting cytidine (**1**) with lauroylchloride in DMF at freezing temperatures. The product was purified via silica gel column chromatography as a crystalline solid. The FTIR spectrum (Fig. 3) of compound **2** showed the following absorption bands: 1710 cm^{-1} (due to –CO), 3410 cm^{-1} (due to –OH), 2830 cm^{-1} (due to –NH), and 2891 cm^{-1} (due to –CH) stretching. In its ^{1}H NMR spectrum (Fig. S1), two two-proton multiplets at δ 2.37{$CH_3(CH_2)_9CH_2CO$-} and δ 1.67 {$CH_3(CH_2)_8CH_2CH_2CO$-}, a sixteen-proton multiplet at δ 1.28 {$CH_3(CH_2)_8CH_2CH_2CO$-} and a three-proton multiplet at δ 0.88 {$CH_3(CH_2)_{10}CO$-} were due to the presence of one lauroyl group in the molecule. The downfield shifts of the C-5′ proton to δ5.89 (as dd, J = 2.2 and 12.2 Hz, H-5′a) and δ5.84 (as dd, J = 2.3 and 12.3 Hz, H-5′b) from their usual values (~4.00 ppm) (Islam et al., 2023) in precursor compound (**1**) and the resonances of other protons in their anticipated positions revealed the presence of the lauroyl group at position 5'. The formation of 5′-*O*-(lauroyl)cytidine (**2**) might be due to the higher reactivity of the sterically less hindered primary hydroxyl group of the ribose moiety of cytidine **(1)**. The molecular ion peak at *m/z* $[M+1]^+$ 426.48 corresponds to the molecular formula $C_{10}H_{18}O_7$. By complete analysis of the FTIR, ^{1}H NMR, and elemental data, the structure of this compound was assigned as 5′-*O*-(lauroyl)cytidine (**2**). The molecular ion peak at *m/z* [M+1]+ 426.48 corresponds to $C_{12}H_{35}N_3O_6$, as indicated by the ^{13}C NMR (Fig. S6) spectrum.

Table 4
The investigated compounds' HOMOs and LUMOs (1–6) (*iso* value = 0.02 a.u.).

Entry	Optimized structure	HOMO	LUMO
1		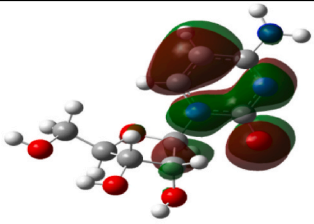	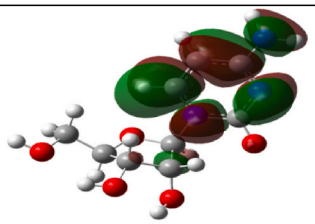
2	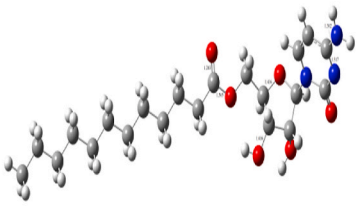	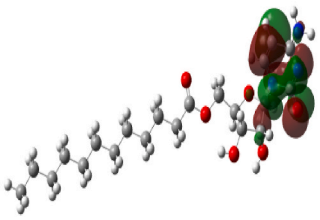	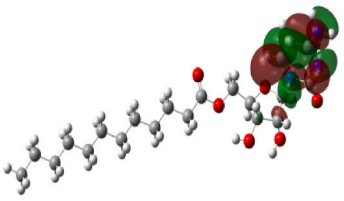
3	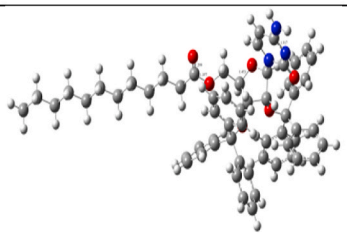	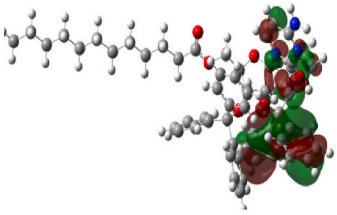	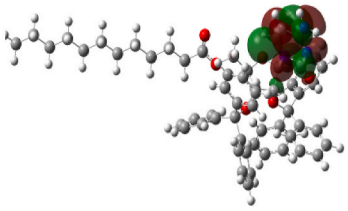
4	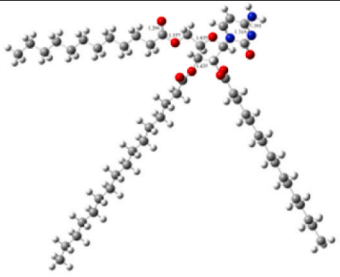	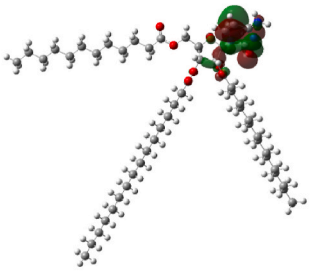	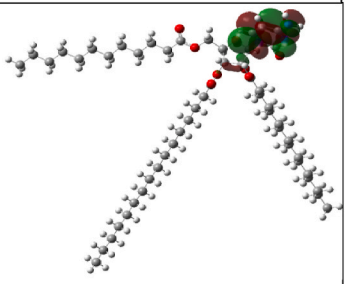
5	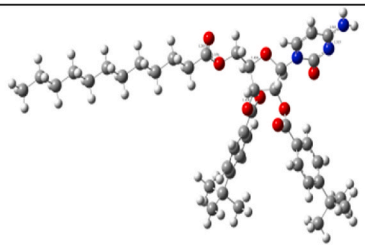	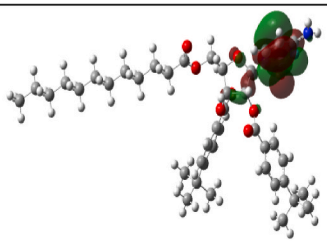	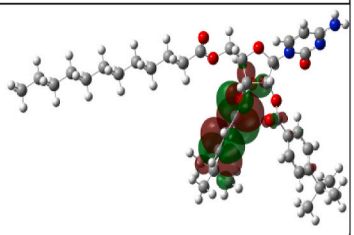
6	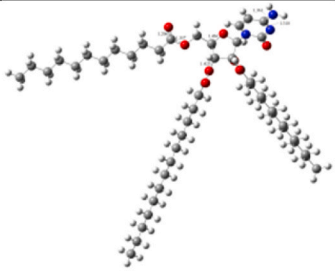	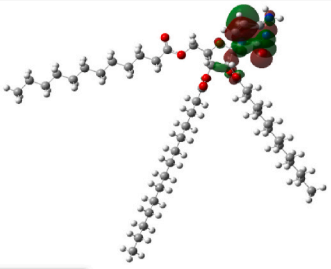	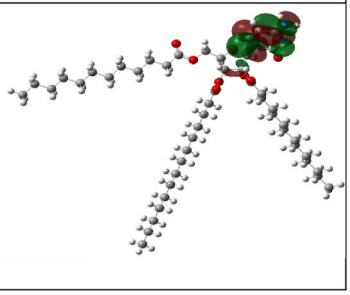

Table 5
Prediction of the antimicrobial activity of compounds via PASS.

Entry	Antimicrobial activity					
	Antibacterial		Antifungal		Antioxidant	
	Pa	Pi	Pa	Pi	Pa	Pi
1	0.395	0.031	0.345	0.065	0.140	0.115
2	0.397[a]	0.036	0.442	0.041	0.158	0.093
3	0.186	0.131	0.337	0.067	0.00	0.00
4	0.392	0.032	0.484	0.033	0.137	0.119
5	0.275	0.070	0.493[a]	0.043	0.173[a]	0.076
6	0.392	0.032	0.484	0.033	0.137	0.119

[a] Found to be actual in vitro potent molecules.

The structure of compound (**2**) was further confirmed by the preparation of its trityl derivative (**3**). Thus, the treatment of compound **2** with triphenylmethyl chloride was followed by a usual work-up and chromatographic purification. The FTIR spectrum of this compound (Fig. 3) revealed a band at 1711 cm^{-1} for –CO stretching, and there was no –OH stretching. In its ^{1}H NMR spectrum (Fig. S2), two characteristic peaks, a twelve-proton triplet at δ 7.35 (2 × Ar–H)) and an eighteen-proton triplet at δ 7.31 (2 × Ar–H), were due to the two triphenylmethyl(trityl) groups in the molecule. The downfield shift of H-2′proton to δ6.01 (as d, $J = 3.3$ Hz) and H-3′proton to δ5.78 (as dd, J = 3.5 and 5.5 Hz) from the values of precursor compound **2** (δ 4.41 and 4.32) confirmed the presence of the triphenyl methyl groups at positions 2′ and 3′. The rest of the protons resonated at their anticipated positions, which led us to propose the structure of this compound as 5′-*O*-lauroyl-2′,3′-di-*O*-(trityl)cytidine (**3**) (Fig. S7).

When the lauroyl derivative **2** was reacted with an equimolar quantity of palmitoyl chloride, 4-*t*-butylbenzoyl chloride, and myristoyl chloride at freezing temperatures, followed by standard procedures and purification *via* column chromatography, the palmitoyl **4**,4-*t*-butylbenzoyl **5** and myristoyl **6** derivatives were obtained in good yields. The structures of the synthesized derivatives 5′-*O*-lauroyl-2′,3′-di-*O*-(palmitoyl)cytidine (**4**) (Figs. S3 and S8), 2′,3′-di-*O*-(4-*t*-butylbenzoyl)-5′-*O*-(lauroyl)cytidine (**5**) (Figs. S4 and S9) and 5′-*O*-lauroyl-2′,3′-di-*O*-(myristoyl)cytidine (**6**) (Figs. S5 and S10) were confirmed by analyzing their FTIR, ^{1}H NMR, and ^{13}C NMR spectra and elemental data.

3.2. Antibacterial efficacy

Synthetic cytidine derivatives (Scheme 1) were screened for their antibacterial properties against several bacterial pathogens, as shown in Table 1. Compounds **2** and **4** demonstrated considerable inhibitory zones against *B. cereus* (12.75 ± 1.0 mm and 8.50 ± 0.5 mm) and *B. subtilis* (11.20 ± 1.1 mm and 8.00 ± 0.5 mm), respectively, according to the test findings (Fig. 4). Compounds **1**, **5**, and **6** had no effect on gram-positive organisms. Moreover, compounds **2** and **5** displayed encouraging outcomes against *S. typhi*, whereas compound **4** generated a moderate inhibitory zone (10.50 ± 0.5 mm). Compound **2** additionally showed good inhibition (13.00 ± 0.5 mm) against *E. coli*. Compounds **4** and **5** revealed unique action at 12.50 ± 0.5 mm and 14.75 ± 0.50 mm, respectively, whereas compound **2** showed a respectable level of inhibition against the gram-negative bacteria *P. aeruginosa* (Fig. S11), which

Table 6(c)
Oral bioavailable parameters of cytidine and its derivatives (**1–6**).

Compound	Molecular weight (g/mol)	LogPo/w (XLOGP3)	No. of H-bond donors	No. of H-bond acceptors	Topological Polar surface area (TPSA) Å^2
1	243.22	−2.13	6	4	130.83
2	426.48	3.20	7	3	130.85
3	912.48	5.63	8	1	142.99
4	903.47	6.09	8	1	142.99
5	746.96	5.12	7	1	131.97
6	847.48	5.87	6	3	136.90

Table 6(a)
Predictions of the pharmacokinetic properties of synthesized compounds via SwissADME.

Entry	Pharmacokinetics								
	GI absorption	BBB permeant	P-gp substrate	CYP1A2 inhibitor	CYP2C19 inhibitor	CYP2C9 inhibitor	CYP2D6 inhibitor	CYP3A4 inhibitor	Log Kp (skin permeation)
1	Low	No	No	No	No	No	No	No	−9.30 cm/s
2	High	No	Yes	No	No	No	No	Yes	−6.56 cm/s
3	Low	No	Yes	No	No	No	No	No	−2.13 cm/s
4	Low	No	Yes	No	No	No	No	No	2.00 cm/s
5	Low	No	Yes	No	No	No	No	Yes	−2.73 cm/s
6	Low	No	Yes	No	No	No	No	No	0.80 cm/s

Table 6 (b)
Drug-likeness attributes of the synthesized cytidine derivatives.

Drug likeness					
Entry	Lipinski	Ghose	Veber	Egan	Muegge
1	Yes; 0 violation	No; 1 violation: WLOGP < −0.4	Yes; 0 violation	Yes; 0 violation	No; 1 violation: XLOGP3<−2
2	Yes; 0 violation	Yes; 0 violation	No; 1 violation: Rotors>10	No; 1 violation: TPSA>131.6	Yes; 0 violation
3	No; 2 violations: MW > 500, MLOGP>4.15	No; 4 violations: MW > 480, WLOGP>5.6, MR > 130, #atoms>70	No; 1 violation: Rotors>10	No; 1 violation: WLOGP>5.88	No; 4 violations: MW > 600, XLOGP3>5, #rings>7, Rotors>15
4	No; 3 violations: MW > 500, MLOGP>4.15, NorO>10	No; 4 violations: MW > 480, WLOGP>5.6, MR > 130, #atoms>70	No; 2 violations: Rotors>10, TPSA>140	No; 2 violations: WLOGP>5.88, TPSA>131.6	No; 3 violations: MW > 600, XLOGP3>5, Rotors>15
5	No; 3 violations: MW > 500, MLOGP>4.15, NorO>10	No; 4 violations: MW > 480, WLOGP>5.6, MR > 130, #atoms>70	No; 2 violations: Rotors>10, TPSA>140	No; 2 violations: WLOGP>5.88, TPSA>131.6	No; 3 violations: MW > 600, XLOGP3>5, Rotors>15
6	No; 3 violations: MW > 500, MLOGP>4.15, NorO>10	No; 4 violations: MW > 480, WLOGP>5.6, MR > 130, #atoms>70	No; 2 violations: Rotors>10, TPSA>140	No; 2 violations: WLOGP>5.88, TPSA>131.6	No; 3 violations: MW > 600, XLOGP3>5, Rotors>15

Table 7
Predictions of the toxicity of the synthesized compounds via Osiris.

Compound	Mutagenic	Tumorigenic	Irritant	Reproductive effective
1				
2				
3				
4				
5				
6				

Nontoxic: ( ), highly toxic: ( ), slightly toxic: ( )

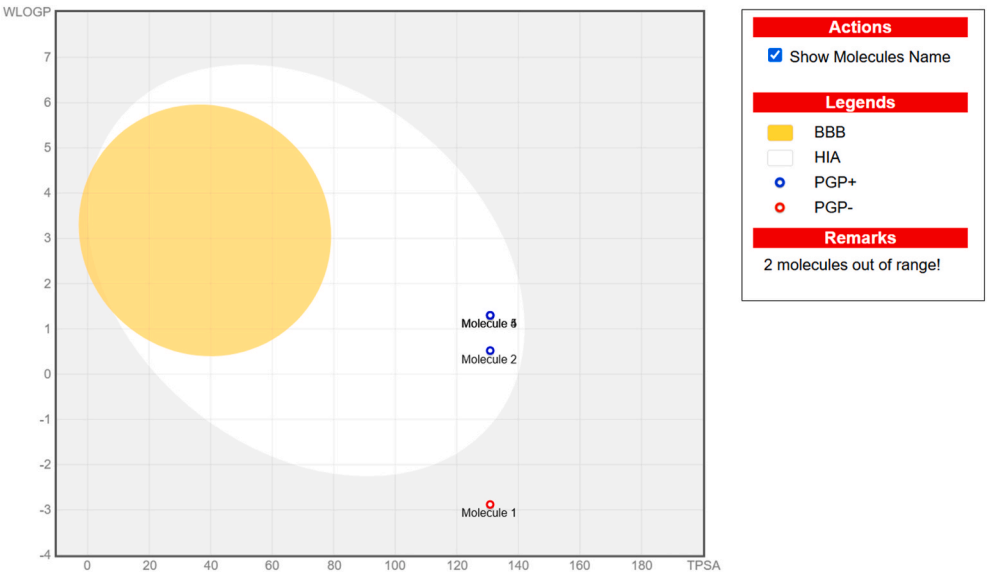

Fig. 10. Boiled egg diagram of compounds (**1–6**).

is compatible with our previous investigations (Kawsar et al., 2018).

3.2.1. MIC and MBC screening

On the basis of its antibacterial accomplishments, compound **2** has shown noteworthy activity against both gram-positive and gram-negative microorganisms. In support of this, compound **2** was scrutinized to find the MIC and MBC further. The MIC values demonstrated that the compound had a minimum MIC value of 8.00 mg/L in the case of *S. typhi* and provided a similar value of 16 mg/L against the other four bacteria. Fig. 5 displays a graphical representation of the MIC test results.

After the MIC of compound **2** was determined, the MBC was also ascertained for all five tested species. For this compound, the MBC was 32 mg/L against all five pathogens. The MBC value curve of the bacteria is shown in Fig. 6.

3.3. Antifungal activity of cytidine derivatives

In this study, the antifungal activities of five cytidine derivatives were evaluated against two fungal strains, *A. flavus* and *A. niger* (Table 2). Significant antifungal activity was demonstrated by compound **5**, with inhibition rates of 78.28 ± 1.0 % against *A. flavus* and 69.07 ± 1.1 % against *A. niger* (Fig. S12). Compounds **1**, **3**, and **6** showed no inhibition (NI) against either fungal strain, indicating a lack of antifungal activity. In contrast, cytidine derivatives **2** and **4** exhibited moderate inhibitory effects on both fungal strains. This study used the standard antifungal agent nystatin as a control. Notably, superior antifungal activity to that of nystatin was shown by compound **5** (4-*t*-butylbenzoyl derivative), indicating its potential as a more effective antifungal agent (Fig. 7) (Kabir et al., 2008).

3.4. DFT studies of the investigated compounds

The data in Table 3 provides a detailed overview of the electronic properties and reactivities of the synthesized compounds, as assessed through various quantum chemical descriptors. The energy of the highest occupied molecular orbital (E_{HOMO}) ranges from −6.3248 eV to −6.5718 eV, reflecting the electron-donating capability of the molecules; higher E_{HOMO} values indicate better potential for nucleophilic behavior. Conversely, the energy of the lowest unoccupied molecular orbital (E_{LUMO}) varies from −1.2017 eV to −1.6328 eV, with more negative values suggesting a greater ability of the molecules to accept

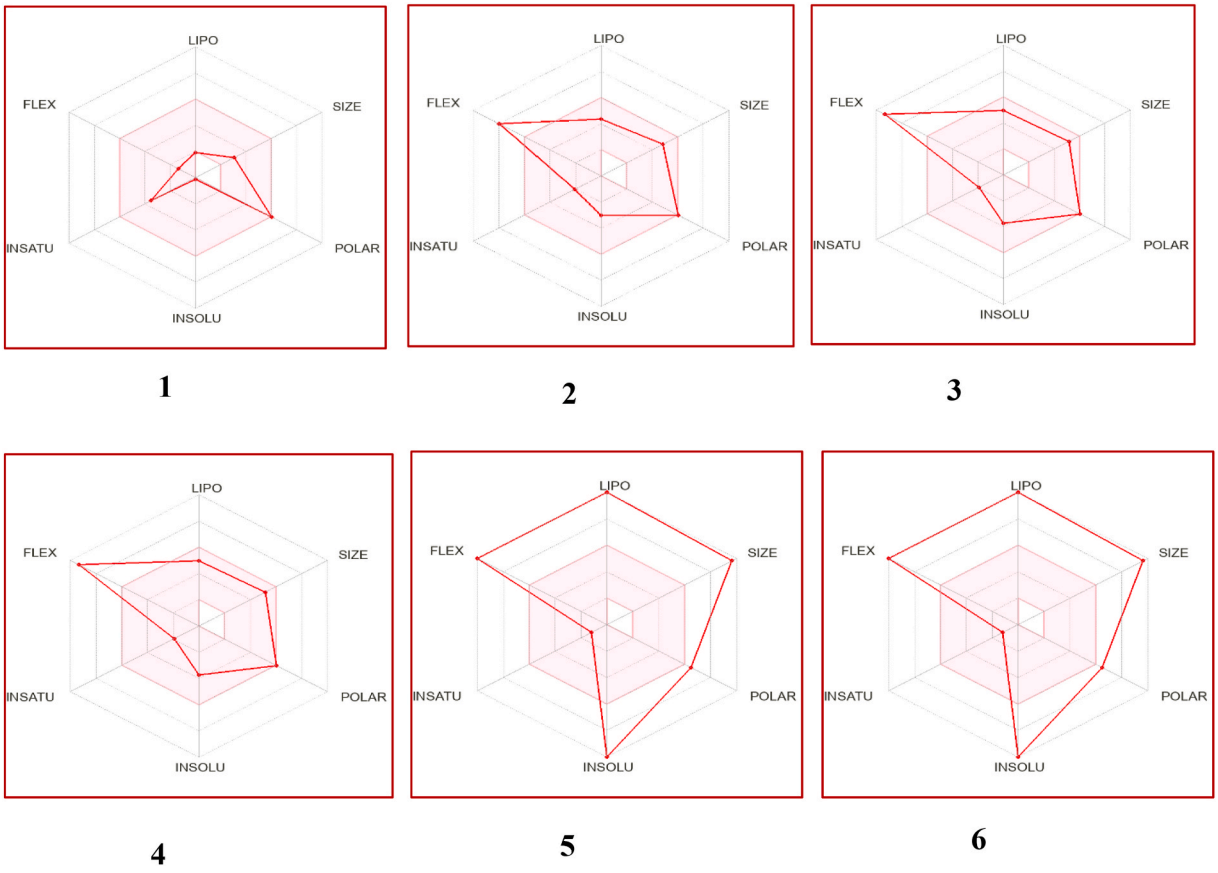

Fig. 11. Swiss ADME - bioavailability radar models of compounds (**1–6**).

electrons, thus indicating their electrophilic potential. The B3LYP-optimized geometries of the compounds under study are illustrated in Table 4. Additionally, the frontier molecular orbitals of the compounds were analyzed in this investigation. As depicted in Table 4, the transition from the HOMO to the LUMO for all title compounds belongs to the π^* transition. However, for **3** and **5**, it is mixed with a charge transfer.

The dipole moment values range from 3.1943 Debye to 9.2900 Debye, highlighting differences in molecular polarity, which affects interactions and reactivity. Chemical hardness (η), spanning from 2.4197 eV to 2.6438 eV, measures the resistance of the compounds to changes in electron density, with lower values indicating higher reactivity and less stability (compound **5**). In contrast, chemical softness (S), ranging between 0.3782 eV^{-1} and 0.3904 eV^{-1}, reflects the susceptibility of the compounds to electron density changes, with higher values suggesting greater reactivity.

The global electrophilicity index (ω) varies from 2.7643 eV to 3.3926 eV, indicating the extent to which the compounds are likely to act as electrophiles in chemical reactions. These parameters collectively reveal the electronic characteristics of the novel derivatives, providing insights into their potential reactivity and interactions (Karthikeyan et al., 2018; Roy et al., 2005). Compounds with higher E_{HOMO} and lower E_{LUMO} values are more likely to participate in nucleophilic and electrophilic reactions, respectively, whereas those with higher dipole moments and lower chemical hardness values show significant polarity and reactivity trends.

Not only the abovementioned dipole moment, softness, hardness, and electrophilic index but also the energy gaps ($\Delta E = E_{LUMO}$-E_{HOMO}) of molecules can serve as reactivity descriptors for comparing the reactivities of molecules. The HOMO–LUMO gap is a key parameter in FMO theory, as it directly correlates with the chemical reactivity of a molecule. The smaller the energy gap a molecule has, the greater its reactivity. The ΔE values in eV are summarized in Fig. 8. As shown in Fig. 8, compound **5** should exhibit the highest chemical reactivity due to its high HOMO energy (−6.47 eV), low LUMO energy (−1.63 eV), and small Egap (4.84 eV). On the other hand, compound **2** should have the lowest reactivity due to having the largest Egap (5.28 eV) among the studied cytidine derivatives. Other compounds **3**, **4**, and **6** should have shown moderate reactivity.

3.5. *Analysis of the molecular electrostatic potential (MEP)*

MEP maps were generated for cytidine (**1**) and its derivatives (**2**–**6**) via the full density matrix. The analysis revealed the distribution of electrostatic potential across the molecular surfaces of these compounds. This electrostatic mapping provides insight into the reactivity and interaction profiles of cytidine derivatives, which are essential for predicting their biological behavior and potential interactions in various applications. In this study, MEPs were calculated via the Multiwfn program and then viewed and saved as an image file by the VMD program (Lu and Chen, 2012; Humphrey et al., 1996). As depicted in Fig. 9, compound **5** should be the most nucleophilic, whereas compounds **4** and **6** should be the most electrophilic. However, the frontier orbitals of the studied molecules indicated that nucleophilic or electrophilic attack of these molecules occurs mainly in their 4-aminopyrimidin-2-one moieties and around the aliphatic chain and benzene ring. The discrepancy between the results of the frontier orbital and those of the MEP might be because not only electrons but also nuclei contribute to the MEP of a molecule.

3.6. *PASS prediction analysis*

The PASS program predicts over 4000 biological activities, both drug and nondrug, with 90 % accuracy. It identifies likely targets and classifies results as Pa (probability of activity) or Pi (probability of

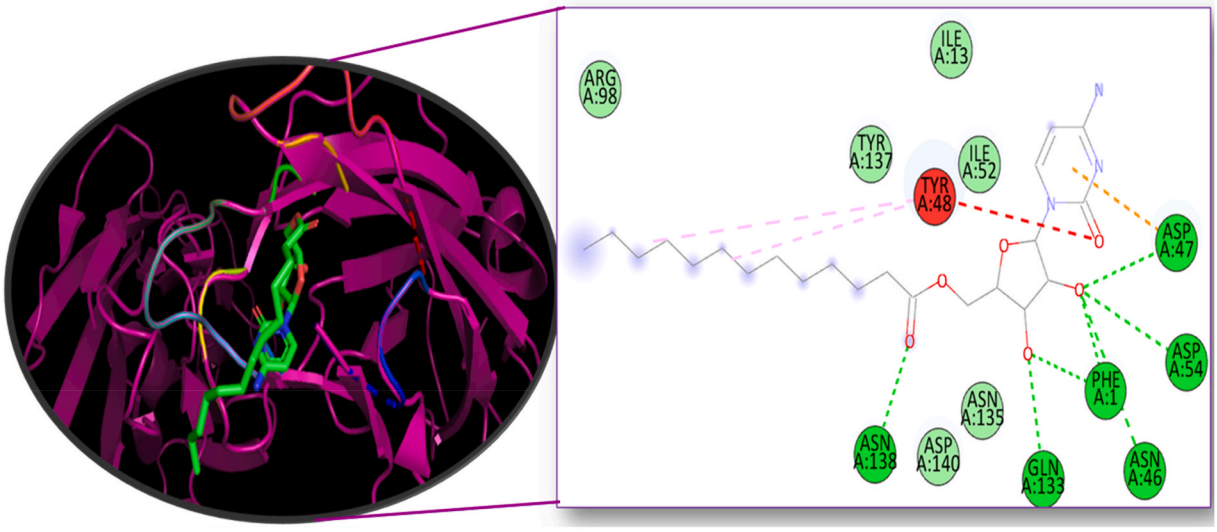

Compound **2**

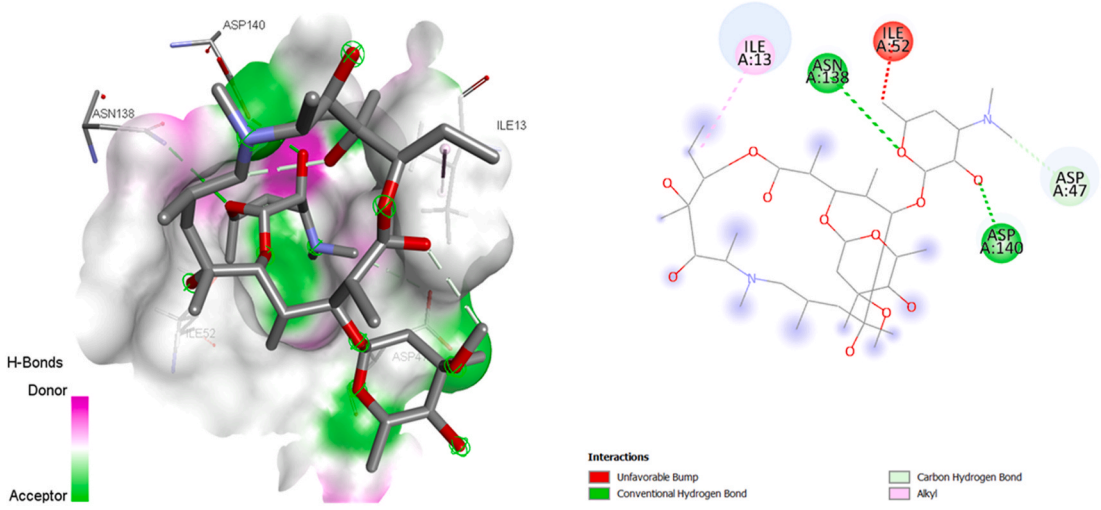

Azithromycin (Std.)

Fig. 12. Docking poses and 2D and 3D interaction diagrams of compound **2** and azithromycin (standard) with 4XO8.

inactivity). A Pa >0.7 suggests a highly active compound, whereas 0.5 < Pa <0.7 indicates lower activity. A Pa <0.5 implies minimal activity. Even if a compound has no known activity, it may still be significant. PASS predictions guide experimental research but can only confirm intrinsic activity through testing. We analyzed the PASS predictions for all the compounds and found good predictions (Table 5). The analysis revealed that compound 2 had a greater probability of being active (0.0397) as an antibacterial agent. In contrast, compound **5** retained a greater probability of acting as an antifungal (0.493) or antioxidant (0.173) agent.

3.7. In silico ADME analysis and toxicity analysis via Osiris calculation

Cytochrome enzymes, particularly cytochrome P450 (CYP) enzymes, play critical roles in the metabolism of drugs, toxins, and endogenous compounds. They are primarily involved in oxidation reactions, transforming lipophilic substances into more water-soluble forms for easier elimination from the body. Found mostly in the liver, CYP enzymes metabolize a wide range of substances, influencing drug efficacy and toxicity. They also help synthesize cholesterol, steroid hormones, and fatty acids. Variations in CYP enzyme activity among individuals can affect drug responses and interactions, making them essential in pharmacology and personalized medicine (Zhao et al., 2021; Hassan et al., 2024). Tables 6(a) and 6(b) clearly indicate that compounds **1**–**6** may not be inhibitors of enzymes such as CYP1A2, CYP2C19, CYP2C9, and CYP2D6. However, we obtained a mixed profile for CYP3A4 inhibition. Candidatures **1** and **2** had no violations for Lipinkis' rule of 5. All of these compounds are nonpermeant to the blood–brain barrier. However, with the exception of compound **2,** all the other molecules presented lower GI absorption profiles.

According to Table 6(c), compounds **1** and **2** partially comply with the rule of five (Ro5) but exceed the limit for hydrogen bond donors (HBD >5), which may hinder oral bioavailability. Compounds **3**, **4**, **5**, and **6** violate multiple Ro5 criteria, including high molecular weight (>500 g/mol), excessive lipophilicity (LogP >5), and too many hydrogen bond donors (HBD >5). The TPSA values are within

Table 8
Molecular docking scores and interactions of synthesized compounds against 4XO8 via iGEMDOCK and PyRx software.

Ligand	Ligand–protein interactions (amino acid residues)	Docking score (kcal.mol^{-1})[a]	Docking score (kcal. mol^{-1})**
1	ASP A:140; ASN A:138; ASN A:135; GLN A:133; ASP A:54; ASN A:46; PHE A:1; ASP A:47 (H-Bonding); ILE A:13 (Pi-Alkyl)	−98.4232	−9.01
2	ASN A:138; GLN A:133; ASP A:54; ASN A:46; PHE A:1; ASP A:47 (H-Bonding); TYR A:48 (Pi-Alkyl)	−115.318	−9.32
3	ALA A:2; PRO A:12; ILE A:13; ILE A:52(Pi-Alkyl)	−71.0803	−7.13
4	ALA A:2; HIS A:45; TYR A:48 (Pi-Alkyl); ILE A:13	−0.764759	−2.35
5	ASN A:138; PHE A:1 (H-Bonding); HIS A:45; ARG A:98; TYR A:48 ((Pi/Alkyl-Alkyl))	−112.456	−9.18
6	PRO A:12; HIS A:45; GLU A:50; ASN A:138; ASP A:140; PHE A:142; PHE A:1 (van der Waals); ALA A:2 (Pi-Alkyl)	−23.4229	−5.68
Azithromycin	ILE A:13 (Alkyl); ASN A:138; ASP A:140 (H-Bonding); ASP A:47 (C–H Bonding)	−79.7366	−7.89

[a] Docking score calculated by 'iGEMDOCK'; ** Docking score calculated by 'PyRx'.

Table 9
Molecular docking scores and interactions of synthesized compounds with IR4U via iGEMDOCK and PyRx software.

Ligand	Ligand–Protein Interactions (Amino Acid residues)	Docking Score (kcal.mol^{-1})[a]	Docking Score (kcal. mol^{-1})**
1	PHE A:258; HIS A:256; ASN A:254; LYS A:171(H-Bonding); ARG A:176 (Pi-Cation); LEU A:170 (Pi-Alkyl)	−92.237	−6.32
2	LYS A:171 (Pi-Alkyl); HIS A:256 (H-Bonding); ILE A:177 (Pi-Lone Pair); ASN A:254 (Acceptor-Acceptor)	−110.361	−7.89
3	TRP A:160; LYS A:171; LEU A:170; ARG A:176; ILE A:177 (Pi-Alkyl)	−82.023	−7.32
4	ILE A:177 (Pi-Alkyl); TYR A:173 (H-Bonding)	71.9171	−6.98
5	THR A:173; LEU A:170; PHE A:258; LEU A:178; LEU A:287; GLN A:228 (van der Waals); PHE A:159; ILE A:288; ILE A:177 (Pi-Pi Hydrophobic); ARG A:176; ASN A:254 (H-Bonding); HIS A:256	−119.145	−8.65
6	PHE A:162; PHE A:159; LEU A:178 (Pi-Alkyl); HIS A:256 (H-Bonding)	−41.2016	−3.67
Fluconazole	THR A:173; LEU A:170 (Pi-Sigma); HIS A:256; ILE A:177 (H-Bonding); PHE A:258; ARG A:176 (H-Bonding)	−84.046	−6.69

[a] Docking score calculated by 'iGEMDOCK'; ** Docking score calculated by 'PyRx'.

acceptable limits for most compounds, except for compounds **3** and **4**, which slightly exceed 140 Å^2. The high molecular weight and excessive number of H-bond donors in compounds **3**–**6** make them poor candidates for oral bioavailability. Structural optimization is recommended to improve drug-likeness and adherence to the Ro5 criteria.

The mutagenicity, tumorigenicity, irritancy, and reproductive toxicity of all synthesized compounds were predicted through Osiris. The Osiris toxicity prediction analysis indicated that all the molecules evaluated were nonmutagenic, nontumorigenic, and nonreproductive toxicants (Pires et al., 2015). However, with the exception of compound **5**, all other molecules were also predicted to be nonirritants (as shown in Table 7).

The analysis of the BOILED-egg diagram, as illustrated in Fig. 10, indicates that the compound lies within the acceptable range for standard drug-like molecules, with its position suggesting potential for central nervous system (CNS) penetration. The white region represents the physicochemical space where molecules have the highest likelihood of being absorbed by the gastrointestinal tract. The yellow region represents the physicochemical space where molecules most likely penetrate the brain. The gray region indicates molecules that may have poor absorption ability and limited ability to cross the blood–brain barrier. The red region signifies the ability to remain in the brain. As shown in Fig. 11, which are in the white region, these compounds align well with the criteria and have good bioavailability (Jayavel et al., 2024a,b).

The bioavailability radar graph provides a comprehensive overview of the drug-likeness and potential bioavailability of a molecule. The radar graph evaluates six key physicochemical properties: lipophilicity (LIPO), size (SIZE), polarity (POLAR), insolubility (INSOLU), saturation (INSATU), and flexibility (FLEX). The profile of the molecule falls within the pink region of the radar graph, which means that the compound meets the optimal ranges for key properties, which are essential for good oral bioavailability. Appropriate lipophilicity and polarity ensure efficient membrane permeability, whereas optimal size and solubility support absorption and distribution. The radar graph thus reflects the potential bioavailability of a molecule by highlighting its adherence to or deviation from the ideal physicochemical space for drug-like compounds (Jayavel et al., 2024a,b). Fig. 11 shows the bioavailability radar graph for all synthesized compounds.

3.8. Molecular docking analysis

FimH is a key target for antivirulence therapies because inhibiting its function can prevent bacterial colonization without exerting selective pressure for antibiotic resistance. This makes it an attractive target for developing novel therapeutics against UTIs caused by multidrug-resistant *E. coli*. Molecular docking This approach aligns with antivirulence strategies to combat infections without promoting antibiotic resistance (Asadi et al., 2019). Urate oxidase is a therapeutic target for the treatment of gout and tumor lysis syndrome. Inhibitors or modulators of this enzyme can help regulate uric acid levels in the body. Additionally, urate oxidase from *A. flavus* is structurally and functionally similar to the human enzyme, making it a suitable model for studying potential inhibitors. The crystal structure of urate oxidase (PDB ID: 1R4U) provides a well-resolved active site, which is essential for molecular docking studies. The tetrameric structure of the enzyme and the availability of cocrystallized ligands make it an excellent candidate for virtual screening and inhibitor design without promoting pathogenesis (Retailleau et al., 2004).

Molecular docking analysis of the 'FimH' lectin domain from *E. coli* K12 indicated that compound **2** was the best-docked candidate (−9.32 kcal/mol). Compound **2** interacts with amino acids such as ASN A:138; GLN A:133; ASP A:54; ASN A:46; PHE A:1; ASP A:47 (H-bonding); and TYR A:48 (Pi-alkyl) (Fig. 12 and S13). Similarly, other compounds also retained amino acids similar to those of compound **2**, indicating the same binding pocket (Table 8). The docking results from both software programs followed the same trend for the docking scores.

Urate oxidase (Uox) from *Aspergillus flavus* plays a key role in purine metabolism by catalyzing the oxidation of uric acid into allantoin, a more soluble and easily excreted compound. This enzyme is crucial for reducing uric acid levels in organisms that lack the ability to metabolize

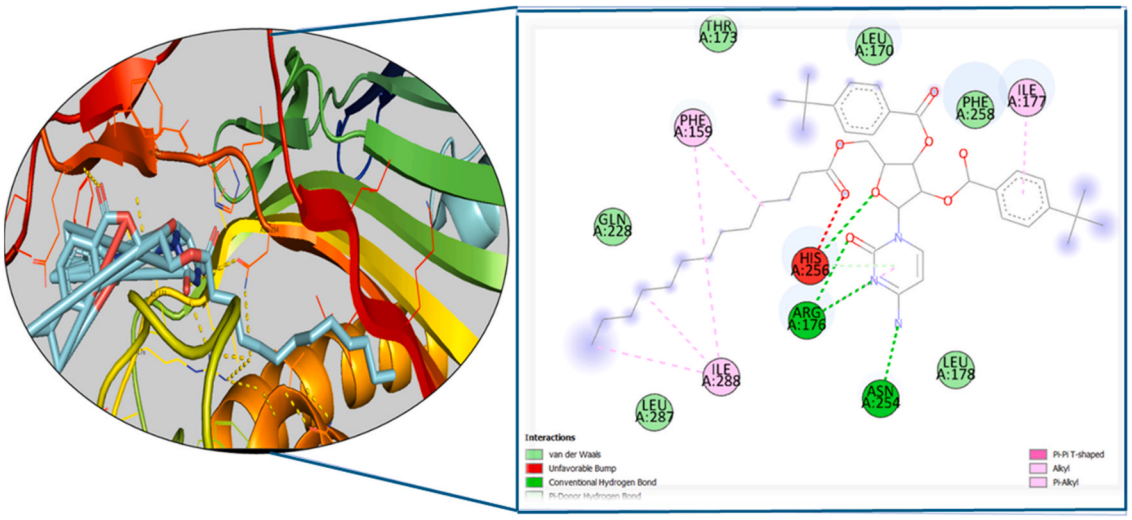

Compound **5**

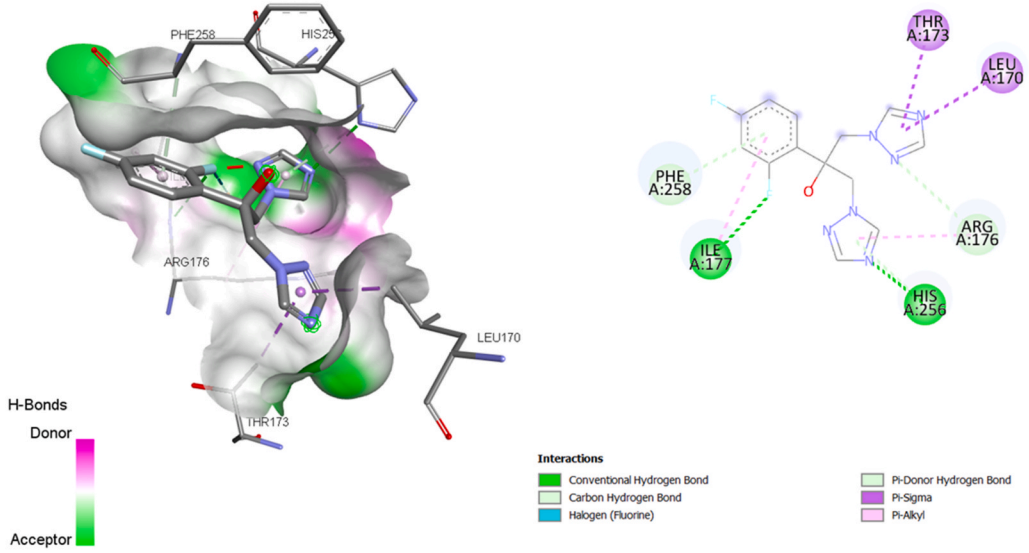

Fluconazole (Std.)

Fig. 13. 2D- and 3D-interaction diagrams of compound **5** and fluconazole (standard) with 1R4U.

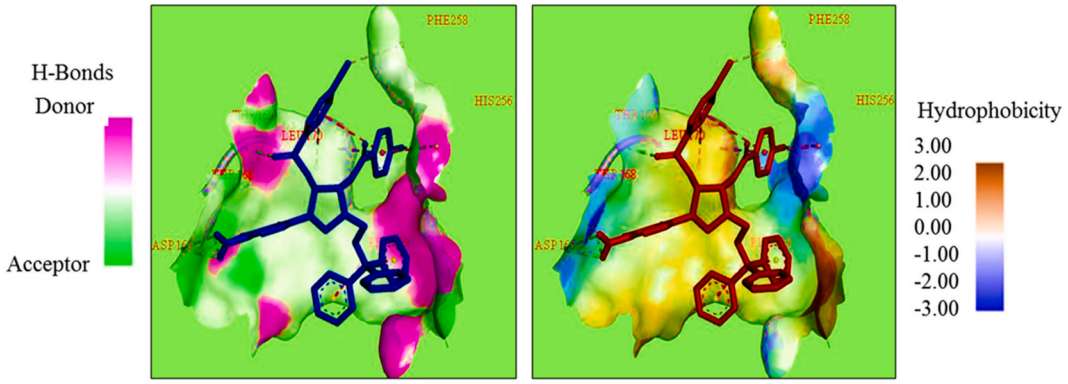

Fig. 14. Compound **5** with a hydrogen bond and hydrophobic surface of 1R4U.

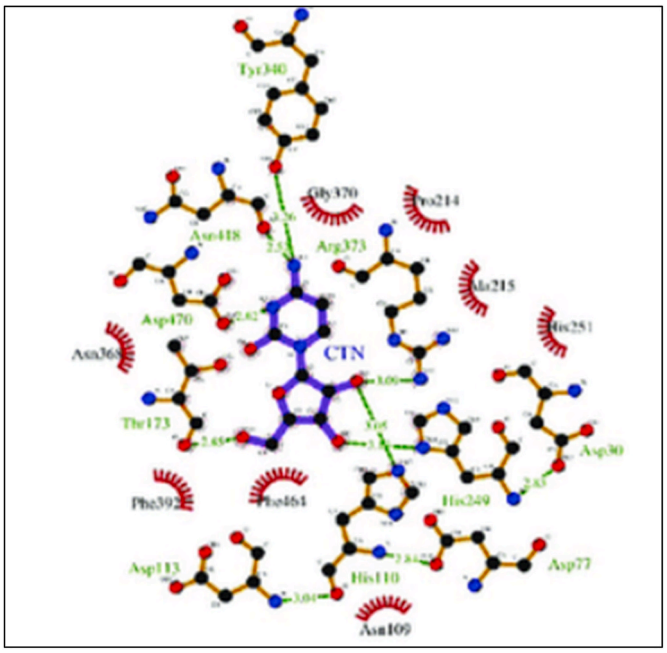

Fig. 15. 2D interaction diagram by LigPlus involving the ligand cytidine.

it efficiently, such as humans. Uox is particularly significant in treating conditions such as hyperuricemia and gout, where excessive uric acid accumulation leads to crystal formation in joints. Table 9 clearly shows that the docking score of compound **5** (docking score: −8.65 kcal/mol) was much better than those of the other compounds. This compound interacted with amino acids such as THR A:173; LEU A:170; PHE A:258; LEU A:178; LEU A:287; GLN A:228 (van der Waals); PHE A:159; ILE A:288; ILE A:177 (Pi-Pi hydrophobic); ARG A:176; ASN A:254 (H-bonding); HIS A:256 (Fig. 13 and S14). The standard fluconazole had interactions with THR A:173; LEU A:170 (Pi-Sigma); HIS A:256; ILE A:177 (H-bonding); PHE A:258; and ARG A:176 (H-bonding), with a docking score of – 6.69 kcal/mol. In addition, compound **5** has a hydrogen bond and hydrophobic surface of 1R4U, which is shown in Fig. 14.

3.9. Molecular dynamics analysis

The targets, the FimH lectin domain (PDB ID: 4XO8) and urate oxidase (PDB ID: 1R4U), along with their best-docked ligands **2** and **5**, respectively, were thus simulated for molecular dynamic (MD) flexibility simulation for a period of 100 ns. Molecular dynamics (MD) simulations analyze ligand–protein complexes in the presence of water, closely mimicking physiological conditions. This detailed analysis helps evaluate the stability of these complexes, providing insights into binding conformations and identifying high-affinity ligand molecules and their optimal protein targets. A 2D interaction diagram by LigPlus involving the ligand cytidine is mentioned in Fig. 15.

3.10. Molecular dynamics trajectory analysis

The root mean square deviation (RMSD) is widely recognized as a key metric for assessing modifications in protein alterations throughout simulations. Moreover, the stability of proteins may be investigated via RMSD analysis. The RMSD readings of the 4XO8:**2** and 1R4U:**5** docked complexes were held at 0.8 and 0.7 nm, respectively. The ligand–protein complex RMSD assessments are shown in Figs. 16 and 17, which were obtained on the basis of the MD simulation findings. The stability of the simulations might also align with the expected connections between various drugs and their human targets, as determined by the MD simulation trials. Additionally, radius of gyration (Rg) analysis was performed, providing information on the stability of the proteins. A stable curve between 2.40 nm and 2.50 nm was created by the Rg values for 100 ns. No discernible deterioration in the compactness of the docked complexes 4XO8:**2** and 1R4U:**5** was observed.

The stabilization of protein–ligand complexes was demonstrated by root mean square fluctuation (RMSF) measurements, which were obtained below reasonable boundaries (0.4 nm and 0.8 nm for 4XO8:**2** and 1R4U:**5**, respectively). Substantial hydrogen bonding engagements involving the chosen binding sites for proteins and the greater affinity ligand were also observed. It was apparent through the examination of the SASA (solvent accessible surface area) statistics that only a handful of 150 and 170 nm^2 regions took place over the whole simulation time of 100 ns. Additionally, more H-bonds were observed, which could account for the increased stability of the bound ligands. Figs. 16 and 17 (a-f) show the overall stabilities of a few chosen ligand–protein pairings on the basis of their RMSD, RMSF, and Rg values.

3.11. Structure–activity relationship (SAR)

A compound's chemical structure and biological activity are related and have been the subject of much research in recent years (Alam et al., 2022; Maowa et al., 2021). Tables 1 and 2 and the PASS prediction in Table 5 clearly indicate that the addition of 4-*t*-butyl benzoyl, lauroyl (C-12), and palmitoyl (C-16) groups increased the antimicrobial activity of cytidine. Table 1 shows that the antibacterial activity of cytidine (**1**) was enhanced by introducing the lauroyl group at the C-5' position and the benzene nucleus (4-*t*-butylbenzoyl group) at the C-2' and C-3' positions to derivative **5**. Derivative **5** has the most activity because it is more hydrophobic than the other derivatives are. In the case of compound **4**, the integration of the palmitoyl group at positions C-2' and C-3', which were already composed of the lauroyl group at position 5', resulted in moderate suppression of the tested pathogens. Moreover, derivatives **2** and **4** were highly efficient against gram-positive and gram-negative bacteria. Compared with other derivatives, derivative **2** (5'-*O*-lauroylcytiidine) showed greater promise, as it presented a lower MIC and MBC, with a greater zone of inhibition against all five bacteria. The lauroyl group ($C_{12}H_{23}CO$-) and the bulky *t*-butylbenzoyl group may increase the ability of a molecule to interact with certain bacterial enzymes or DNA/RNA, influencing the antibacterial spectrum and potency. The hydrophobic nature of the lauroyl chain allows it to integrate into lipid bilayers, potentially disrupting membrane integrity and increasing permeability. The cytidine moiety may interact with bacterial nucleic acids or enzymes, contributing to the antibacterial effect (Munia et al., 2022). According to Hunt's theory, the lipid solubility and potency of aliphatic alcohols are closely correlated because of the hydrophobic contact between the alcohol's alkyl chains and the lipid portion of the membrane (Kawsar et al., 2024b). Owing to their thicker peptidoglycan layers, gram-positive bacteria might be more susceptible to membrane-disrupting agents such as lauroyl derivatives (Fig. 18). Gram-negative bacteria have an outer membrane that can act as a barrier to hydrophobic compounds, potentially reducing the efficacy of these derivatives (Munia et al., 2023). Therefore, a compound's antibacterial activity may be increased by its hydrophobicity and the presence of an aromatic ring.

4. Discussion

In this study, we successfully synthesized an array of cytidine derivatives via a regioselective direct acylation method (Munia et al., 2023; Maowa et al., 2021). This approach resulted in the formation of five unique acylated cytidine derivatives. The IR spectra of the compounds exhibited characteristic hydroxyl and carbonyl stretching vibrations, confirming the successful introduction of acyl groups. NMR and MASS spectra further validated the structures, with significant shifts, corresponding to the aromatic or alicyclic protons of the acyl

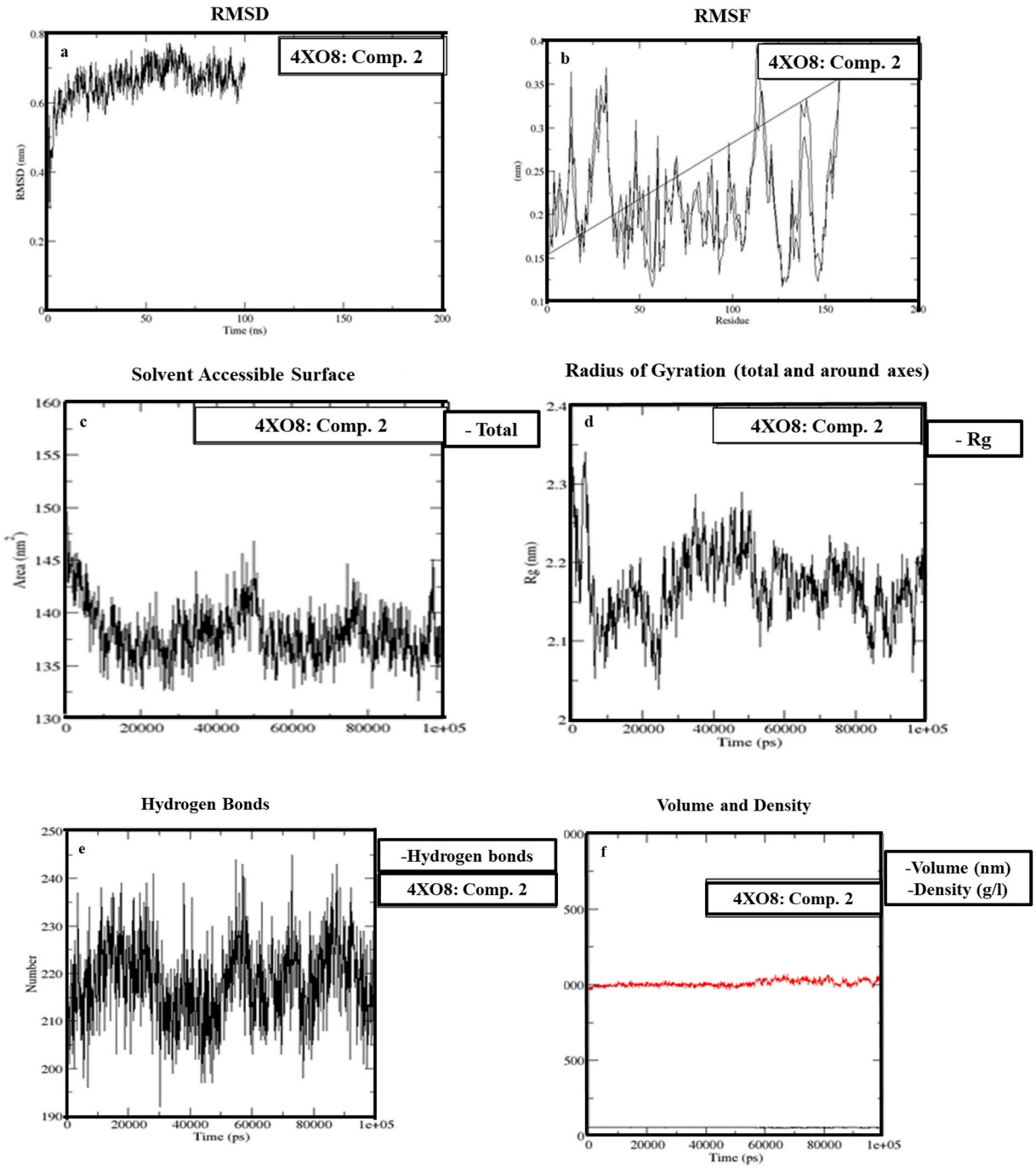

Fig. 16. Analysis of the results of the molecular dynamics simulations (a–f). (a) Root mean square deviation (RMSD) for complex 4XO8:2, (b) root mean square fluctuation (RMSF) for complex 4XO8:**2**, (c) solvent accessible surface area, (d) radius of gyration, (e) number of hydrogen bonds for complex 4XO8:**2** and (f) volume and density analysis.

groups. The antibacterial activity of the synthesized derivatives was evaluated against 2 g-positive bacteria, *B. cereus* and *B. subtilis*, and 3 g-negative bacteria, *E. coli*, *S. typhi*, and *Pseudomonas aeruginosa*. Derivative **5** showed the highest antibacterial activity, with an inhibition zone of 14.75 ± 0.50 mm against *P. aeruginosa* and 13.50 ± 0.5 mm against *S. typhi,* but did not have any activity for gram-positive bacteria, indicating selectivity toward gram-positive bacteria. In contrast, derivative **2** showed significant potency against all five tested bacteria, with a minimum MIC value of 8.00 mg/L against *S. typhi and an* MBC of 32 mg/L against all five pathogens, which is quite similar to the findings of Munia et al. (2022) and Hosen et al. (2022). Furthermore, derivative 4 had moderate activity against 2 g-positive and 2 g-negative bacteria. For antifungal activity, the derivatives were tested against *A. flavus* and *A. niger*. Derivative **5** demonstrated significant antifungal activity, with inhibition rates of 78.28 ± 1.0 % and 69.07 ± 1.1 % against *A. flavus* and *A. niger,* respectively, highlighting its potency as an effective antifungal compound. To further elucidate the properties of the synthesized compounds, density functional theory (DFT) was employed for molecular optimization (Stephens et al., 1994). The computed HOMO–LUMO gap analysis revealed that acylation significantly affects the electronic properties of cytidine derivatives (Tabassum et al., 2024; Pal and Chattaraj, 2021). Among the tested compounds, Compound **5** exhibited the lowest chemical hardness, indicating high reactivity and low chemical stability. Conversely, the opposite results were obtained for

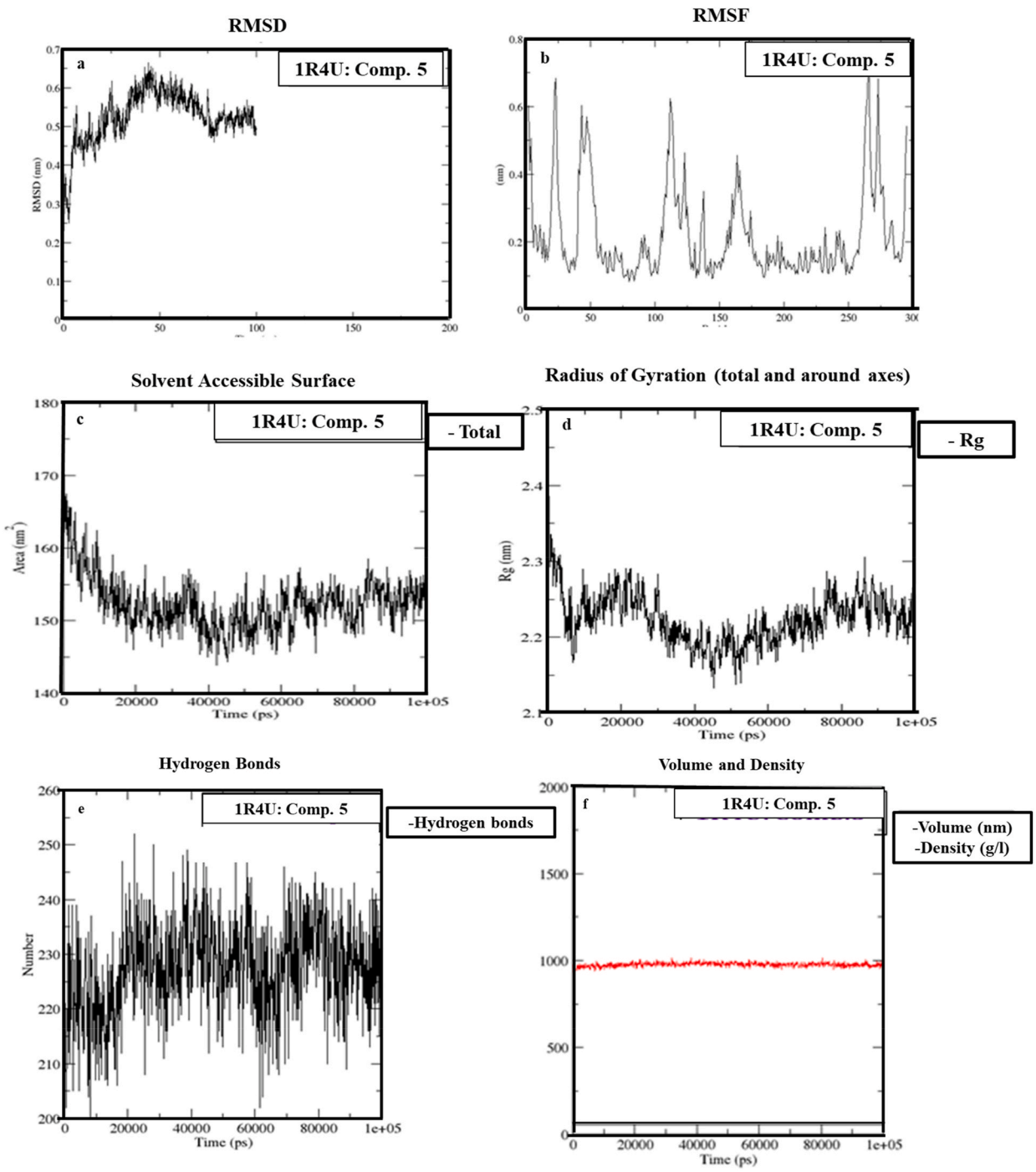

Fig. 17. Analysis of the results of the molecular dynamics simulations (a–f). (a) Root mean square deviation (RMSD) for complex 1R4U:**5**, (b) root mean square fluctuation (RMSF) for complex 1R4U:**5**, (c) solvent accessible surface area, (d) radius of gyration, (e) number of hydrogen bonds for complex 1R4U:**5** and (f) volume and density analysis.

Compound **2**, which demonstrated greater stability and lower reactivity. Potential reactive sites were identified via molecular electrostatic potential (MEP) analysis (Breneman and Martinov, 1996). The MEP analysis revealed moderate electron density in the aromatic ring structures and increased electron density surrounding the 4-aminopyrimidin-2-one units, indicating potential locations of interactions with biological targets. To evaluate the binding affinities of synthesized compounds (**1**–**6**) with two target proteins, the FimH lectin domain from *E. coli* K12 (PDB ID: 4XO8) and urate oxidase from *Aspergillus flavus* (PDB ID: IR4U), molecular docking techniques were subsequently utilized. Using iGEMDOCK and PyRx for simulations, the study revealed that compounds **2** and **5** were the most promising inhibitors for both target proteins and exhibited strong binding affinities and significant interactions, such as hydrogen bonding and π−alkyl interactions. Comparative analysis with the reference drugs azithromycin and fluconazole revealed that these standard drugs had weaker binding affinities, highlighting the superior potential of compounds **2** and **5** as effective inhibitors of FimH and urate oxidase, respectively. The molecular dynamics simulations for the FimH lectin domain (4XO8) with ligand **2** and urate oxidase (1R4U) with ligand **5** demonstrated distinct stabilities, reflected by RMSD values maintained below 0.8 nm and 0.7 nm, respectively. The radius of gyration (Rg) analysis confirmed protein

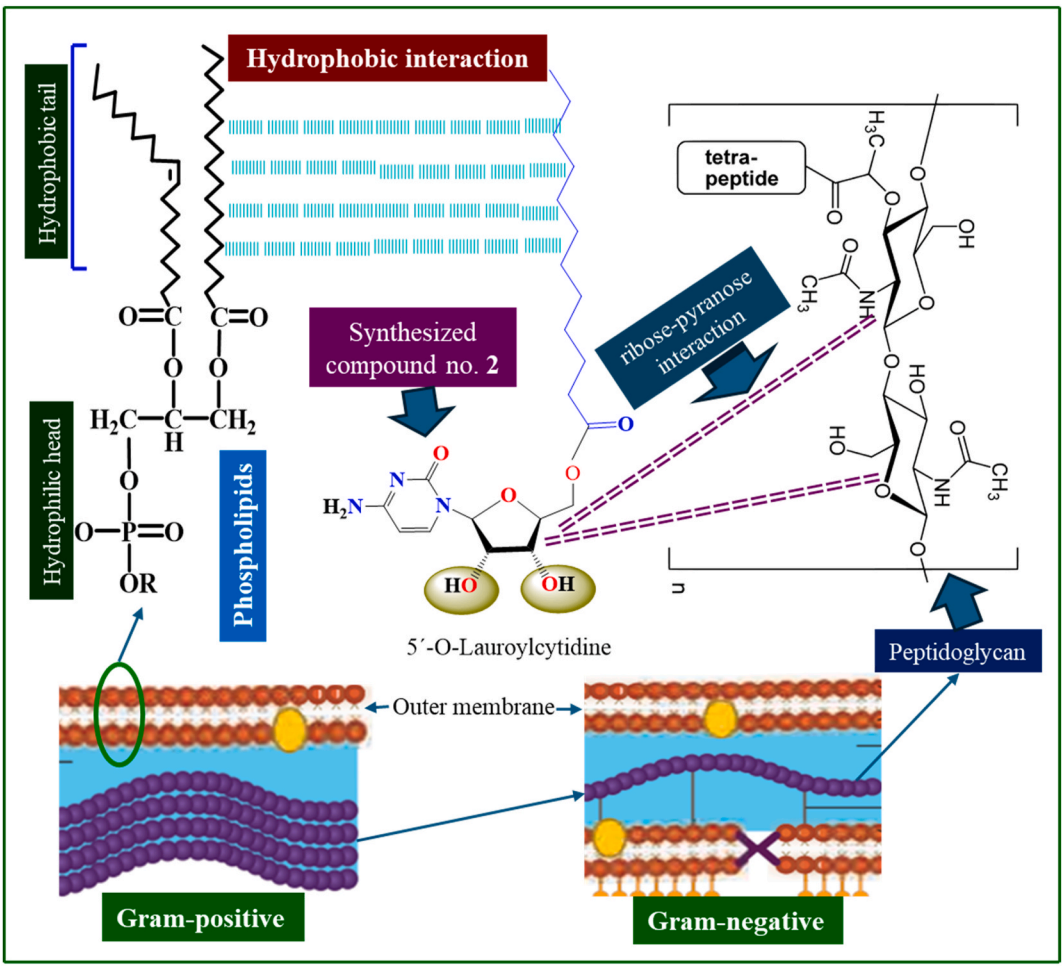

Fig. 18. Structure–activity relationships of synthesized cytidine derivatives.

compactness, with stable values between 2.40 nm and 2.50 nm throughout the 100 ns simulation. The RMSF values remained within acceptable limits, demonstrating the stability of the protein–ligand complexes. The significant hydrogen bonding interactions and consistent solvent accessible surface area (SASA) measurements, with minima of 150 nm^2 and 170 nm^2 for 4XO8:**2** and 1R4U:**5**, respectively, indicated strong and stable binding affinities. In silico ADMET prediction for cytidine and its derivatives reveals a mixed profile with specific strengths and potential limitations. Compound **2** stands out for its lower GI absorption and notable interactions with CYP3A4 and P-gp, which need further investigation. The high skin permeability of compound 4 suggests an alternative route of administration. Except for compounds **1** and **2,** all the derivatives violated Lipinski's rule of 5. These insights highlight the importance of early ADMET profiling in drug development to optimize the design and selection of promising drug candidates for further in vivo studies. Structure–activity relationship analysis revealed that compounds containing larger acyl (lauroyl and palmitoyl) groups or benzene rings (4-*t*-butylbenzoyl) generally exhibited greater antibacterial activity. For example, compounds **2** and **4**, with a bulky acyl group at the 5′ position in the cytidine, showed significant activity compared with the parent cytidine. In the case of compound **5**, the lauroyl group at the 5′ position and two 4-*t*-butylbenzoyl groups at the 2′ and 3′ positions exhibited robust potential against 2 g-negative bacteria and two tested fungi. The prediction of biological activity was performed via the Prediction of Activity Spectra for Substances (PASS) software, which provided insights into the potential biological activities of the derivatives beyond the tested pathogens (Filimonov et al., 2014). PASS predictions also supported this in vitro analysis. These findings suggest that large aliphatic chains or aromatic rings may increase binding affinities and biological efficacy. Among the compounds that were assessed, compounds **2** and **5** are the most promising potential antibacterial drug candidates, and compound **4** is relatively more effective, suggesting that it may be a significant option for future antibacterial drug development.

5. Conclusion

In this extensive investigation, we systematically synthesized a series of cytidine derivatives via a regioselective direct acylation technique, yielding five distinct acylated cytidine derivatives. The NMR spectra revealed different chemical shifts that aligned with the expected structural motifs, whereas IR and MASS spectroscopy identified characteristic functional groups, confirming successful synthesis with good yield. The antibacterial and antifungal activities of the synthesized derivatives were rigorously evaluated, revealing significant findings. Notably, compound **2** had more potential than the other derivatives since it had a lower MIC and MBC as well as a larger zone of inhibition against each of the five bacteria. Compound **4** also exhibited moderate antibacterial activity. Compound **5** exhibited the highest antibacterial activity against 2 g-negative bacteria (*S. typhi* and *P. aeruginosa*). Additionally, it also displayed significant antifungal activity against *Aspergillus flavus* and *Aspergillus niger*. SAR evaluations revealed that the insertion of larger alicyclic (e.g., lauroyl and palmitoyl) groups and benzene rings (e.g., 4-*t*-butylbenzoyl) into the cytidine framework significantly affected the biological activity of these compounds. Complementary computational studies, including DFT and FMO studies, have provided deeper insights into the electronic properties and reactivities of the derivatives. The

MEP studies revealed higher electron density around the 4-aminopyrimidin-2-one moieties and moderate electron density in the aliphatic long-chain and aromatic ring groups, indicating potential sites for interactions with biological targets. Molecular docking analysis of the FimH lectin domain from *Escherichia coli* K12 identified compound **2** as the best docking candidate, with a binding affinity of −9.32 kcal/mol, and compound **5**, with a docking score of −8.65 kcal/mol, exhibited strong interactions with urate oxidase (Uox) from *Aspergillus flavus* with stability for 100 ns molecular dynamics, which offered insights into the stability and flexibility of the structural organization around complexes created with cytidine derivatives. Compounds **1** and **2** did not violate Lipinski's rule of 5, whereas all the other compounds were nonpermeant to the blood−brain barrier. Compound **2** displayed a relatively high probability of antibacterial activity, and compound **5** showed potential as an antifungal and antioxidant agent on the basis of PASS analysis. In summary, the lauroyl cytidine derivatives synthesized in this study exhibit substantial antimicrobial activity, as supported by both wet laboratory experiments and computational analyses. The promising pharmacological characteristics and significant antibacterial and antifungal activities of these compounds highlight the possibility of their function as potent antimicrobial agents. To advance these cytidine derivatives toward therapeutic applications, future studies should focus on experimental validation in *in vivo* studies in relevant animal models to assess their efficacy, toxicity, and pharmacokinetics, prioritizing compounds **2** and **5** for their promising antimicrobial activity. Further SAR optimization and toxicity profiling will be essential to increase their therapeutic potential. These experimental validations bridge the gap between computational predictions and practical applications. Preclinical studies, including formulation development and bioavailability assessments, will pave the way for clinical translation.

CRediT authorship contribution statement

Sarkar M.A. Kawsar: Writing – review & editing, Writing – original draft, Validation, Supervision, Project administration, Methodology, Investigation, Conceptualization. **Rahnuma Tabassum:** Formal analysis, Data curation. **Nasrin Sultana Munia:** Writing – original draft, Visualization, Validation. **Suraj N. Mali:** Writing – review & editing, Visualization, Validation, Software. **Chin-Hung Lai:** Writing – original draft, Software, Investigation. **Jannatul Ferdous:** Visualization, Validation, Formal analysis. **Ferdausi Ali:** Validation, Methodology, Investigation.

Funding

This work was supported by Research & Publication Cell, University of Chittagong, Bangladesh [grant number *143/2023–24/3rdcall/10/2024*].

Declaration of competing interest

The authors declare that they have no known competing financial interests or personal relationships that could have appeared to influence the work reported in this paper.

Appendix A. Supplementary data

Supplementary data to this article can be found online at https://doi.org/10.1016/j.amolm.2025.100077.

References

Adkins, J.C., Peters, D.H., Faulds, D., 1997. Zalcitabine: an update of its pharmacodynamic and pharmacokinetic properties and clinical efficacy in the management of HIV infection. Drugs 53 (6), 1054–1080. https://doi.org/10.2165/00003495-199753060-00009.

Akter, N., Saha, S., Hossain, M.A., Uddin, K.M., Bhat, A.R., Ahmed, S., Kawsar, S.M.A., 2024. Acylated glucopyranosides: FTIR, NMR, FMO, MEP, molecular docking, dynamics simulation, ADMET and antimicrobial activity against bacterial and fungal pathogens. Chem. Phys. Impact 9, 100700. https://doi.org/10.1016/j.chphi.2024.100700.

Alam, A., Rana, K.M., Hosen, M.A., Dey, S., Bezbaruah, B., Kawsar, S.M.A., 2022. Modified thymidine derivatives as potential inhibitors of SARS-CoV: PASS, in vitro antimicrobial, physicochemical and molecular docking studies. Phys. Chem. Res. 10 (3), 391–409. https://www.physchemres.org/article_144649.

Arzine, A., Hadni, H., Boujdi, K., Chebbac, K., Barghady, N., Rhazi, Y., Chalkha, M., Nakkabi, A., Chkirate, K., Mague, J.T., Kawsar, S.M.A., 2024. Efficient synthesis, structural characterization, antibacterial assessment, ADME-Tox analysis, molecular docking and molecular dynamics simulations of new functionalized isoxazoles. Molecules 29 (14), 3366. https://doi.org/10.3390/molecules29143366.

Asadi, A., Razavi, S., Talebi, M., Gholami, M., 2019. A review on anti-adhesion therapies of bacterial diseases. Infection 47, 13–23. https://doi.org/10.1007/s15010-018-1222-5.

Balouiri, M., Sadiki, M., Ibnsouda, S.K., 2016. Methods for in vitro evaluating antimicrobial activity: a review. J. Pharm. Anal. 6 (2), 71–79. https://doi.org/10.1016/j.jpha.2015.11.005.

Bauer, A.W., Kirby, W.M., Sherris, J.C., Turck, M., 1966. Antibiotic susceptibility testing by a standardized single disk method. Am. J. Clin. Pathol. 45 (4), 493–496. https://doi.org/10.1093/ajcp/45.4_ts.493.

Becke, A.D., 1993. Density-functional thermochemistry. III. The role of exact exchange. J. Chem. Phys. 98 (7), 5648–5652. https://doi.org/10.1063/1.464913.

Becke, A.D., 1998. Density-functional exchange-energy approximation with correct asymptotic behavior. Phys. Rev. 38, 3098. https://doi.org/10.1103/PhysRevA.38.3098.

Bhuiyan, T.S., Said, M.A., Bulbul, M.Z.H., Ahmed, S., Bhat, A.R., Chalkha, M., Kawsar, S.M.A., 2024. Synthesis, antimicrobial, and in silico studies of c5'-*O*-substituted cytidine derivatives: cinnamoylation leads to improvement of antimicrobial activity. Nucleosides Nucleotides Nucleic Acids 43 (12), 1–39. https://doi.org/10.1080/15257770.2024.2333495.

Bouckaert, J., Berglund, J., Schembri, De Genst, E., Cools, L., Wuhrer, M., Hung, C.S., Pinkner, J., Slättegård, R., Zavialov, A., Choudhury, D., 2005. Receptor binding studies disclose a novel class of high-affinity inhibitors of the *Escherichia coli* FimH adhesin. Mol. Microbiol. 55 (2), 441–455. https://doi.org/10.1111/j.1365-2958.2004.04415.x.

Breneman, C.M., Martinov, M., 1996. The use of electrostatic potential fields in QSAR and QSPR. Theor. Comput. Chem. 3 (1), 143–179. https://doi.org/10.1016/S1380-7323(96)80043-4.

Bulbul, M.Z.H., Chowdhury, T.S., Misbah, M.M.H., Ferdous, J., Dey, S., Hasan, I., Fujii, Y., Ozeki, Y., Kawsar, S.M.A., 2021. Synthesis of new series of pyrimidine nucleoside derivatives bearing the acyl moieties as potential antimicrobial agents. Pharmacia 68 (1), 23–34. https://doi.org/10.3897/pharmacia.68.e56543.

Bulbul, Z.H., Hosen, M.A., Ferdous, J., Chowdhury, T.S., Misbah, M.H., Kawsar, S.M.A., 2021. DFT study, physicochemical, molecular docking, and ADMET predictions of some modified uridine derivatives. J. New. Chem. 8 (1), 88–110. https://doi.org/10.22034/ijnc.2020.131337.1124.

Chowdhury, S.A., Bhuiyan, M.M.R., Ozeki, Y., Kawsar, S.M.A., 2016. Simple and rapid synthesis of some nucleoside derivatives: structural and spectral characterization. Curr. Chem. Lett. 5 (2), 83–92. https://doi.org/10.5267/j.ccl.2015.12.001.

Christaki, E., Marcou, M., Tofarides, A., 2020. Antimicrobial resistance in bacteria: mechanisms, evolution, and persistence. J. Mol. Evol. 88 (1), 26–40. https://doi.org/10.1007/s00239-019-09914-3.

M07: Clinical and Laboratory Standards Institute Methods for Dilution Antimicrobial Susceptibility Tests for Bacteria That Grow Aerobically, Clin. Lab. Stand. Inst. 9. Balouiri, M., Sadiki, M., Ibnsouda, S.K. Clinical and Laboratory Standards Institute (CLSI), 2018, 2016. Methods for in vitro evaluating antimicrobial activity: a review J. Pharm. Anal. 6 (2), 71–79. https://doi.org/10.1016/j.jpha.2015.11.005.

Dennington, Roy, Keith Todd, A., Millam, John M., 2016. GaussView, Version 6. Semichem Inc., Shawnee Mission, KS.

Di Francia, R., Crisci, S., De Monaco, A., Cafiero, C., Re, A., Iaccarino, G., De Filippi, R., Frigeri, F., Corazzelli, G., Micera, A., Pinto, A., 2021. Response and toxicity to cytarabine therapy in leukemia and lymphoma: from dose puzzle to pharmacogenomic biomarkers. Cancers 13 (5), 966. https://doi.org/10.3390/cancers13050966.

Ferri, M., Ranucci, P., Romagnoli, E., Giaccone, V., 2017. Antimicrobial resistance: a global emerging threat to public health systems. Crit. Rev. Food Sci. Nutr. 57 (13), 2857–2876. https://doi.org/10.1080/10408398.2015.1077192.

Filimonov, D.A., Lagunin, A.A., Gloriozova, T.A., Rudik, A.V., Druzhilovskii, D.S., Pogodin, P.V., Poroikov, V.V., 2014. Prediction of the biological activity spectra of organic compounds using the pass online web resource. Chem. Heterocycl. Compd. 50, 444–457. https://doi.org/10.1007/s10593-014-1496-1.

Frisch, M.J., Trucks, G.W., Schlegel, H.B., Scuseria, G.E., Robb, M.A., Cheeseman, J.R., Scalmani, G., Barone, V., Mennucci, B., Petersson, G.A., Nakatsuji, H., Caricato, M., Li, X., Hratchian, H.P., Izmaylov, A.F., Bloino, J., Zheng, G., Fox, J., Sonnenberg, J. L., Hada, M., Ehar, M., Fox, D.J., 2013. Gaussian 09, Revis. E.01. Gaussian, Inc., Wallingford CT.

Fujii, Y., Kawsar, S.M.A., Matsumoto, R., Yasumitsu, H., Naoto, I., Dohgasaki, C., Hosono, M., Nitta, K., Hamako, J., Matsui, T., Ozeki, Y., 2011. A-D-galactose-binding lectin purified from coronate moon turban, *Turbo (Lunella) coreensis*, with a unique amino acid sequence and the ability to recognize lacto-series glycophingolipids. Comp. Biochem. Physiol. 158B (1), 30–37. https://doi.org/10.1016/j.cbpb.2010.09.002.

Gurav, S.S., Waghmode, K.T., Dandekar, S.N., Jadhav, S.D., Lotlikar, O.A., Jadhav, S.R., Mali, S.N., Naphade, J.G., 2024. New 2-Chloroimidazo[1,2-a]pyridine induced Schiff bases: synthesis, characterization, antimicrobial and A-498 and A-549 anticancer activity, molecular modeling, in-silico pharmacokinetics, and DFT studies. Chem. Phys. Impact 8 (1), 100494. https://doi.org/10.1016/j.chphi.2024.100494.

Hantosh, M.N.K., Hassan, K.A., Salim, H.A., Sohail, F.M., 2015. Efficacy of tolerance of bioagents and plant pathogenic fungi to fungicides by food poison technique. Eur. Acad. Res. 2 (12), 15403–15411. https://doi.org/10.1016/j.bioorg.2022.105850.

Hassan, S.A., Aziz, D.M., Abdullah, M.N., Bhat, A.R., Dongre, R.S., Hadda, T.B., Almalki, F.A., Kawsar, S.M.A., Rahiman, A.K., Ahmed, S., Abdellattif, M.H., Berredjem, M., Sheikh, S.A., Jamali, J., 2024. *In vitro* and *in vivo* evaluation of the antimicrobial, antioxidant, cytotoxic, hemolytic activities and in silico POM/DFT/DNA-binding and pharmacokinetic analyses of new sulfonamide bearing thiazolidine-4-ones. J. Biomol. Struct. Dyn. 42 (7), 3747–3763. https://doi.org/10.1080/07391102.2023.2226713.

Hosen, M.A., Munia, N.S., Al-Ghorbani, M., Baashen, M., Almalki, F.A., Hadda, T.B., Ali, F., Mahmud, S., Saleh, M.A., Laaroussi, H., Kawsar, S.M.A., 2022. Synthesis, antimicrobial, molecular docking and molecular dynamics studies of lauroyl thymidine analogs against SARS-CoV-2: POM study and identification of the pharmacophore sites. Bioorg. Chem. 125 (1), 105850. https://doi.org/10.1016/j.bioorg.2022.105850.

Hosen, M.A., Qais, F.A., Chtita, S., Rahman, I.A., Almehdi, A.M., Ali, F., Almalki, F.A., Hadda, T.B., Laaroussi, H., Kawsar, S.M.A., 2023. In silico and POM analysis for potential antimicrobial agents of thymidine analogs by using molecular docking, molecular dynamics, and ADMET profiling. Nucleosides Nucleotides Nucleic Acids 42 (11), 877–918. https://doi.org/10.1080/15257770.2023.2215839.

Hunt, W.A., 1975. The effects of aliphatic alcohols on the biophysical and biochemical correlates of membrane function. Adv. Exp. Med. Biol. 56 (1), 195–210. https://doi.org/10.1007/978-1-4684-7529-6_9.

Humphrey, W., Dalke, A., Schulten, K., 1996. Vmd - visual molecular dynamics. J. Mol. Graph. 14 (1), 33–38. https://doi.org/10.1016/0263-7855(96)00018-5.

Imberty, A., 2011. Bacterial lectins and adhesins: structures, ligands, and functions in Synthesis and Biological Applications of Glycoconjugates. Bentham Science Book 1 (3), 3–11. https://doi.org/10.2174/978160805277611101010003.

Islam, A.U., Serseg, T., Benarous, K., Ahmmed, F., Kawsar, S.M.A., 2023. Synthesis, antimicrobial activity, molecular docking and pharmacophore analysis of new propionyl mannopyranosides. J. Mol. Struct. 1292, 135999. https://doi.org/10.1016/j.molstruc.2023.135999.

Islam, A.U., Hadni, H., Abuzreda, A., Ali, F., Kawsar, S.M.A., 2024. Synthesis, antimicrobial activity, molecular docking, molecular dynamics simulation, and ADMET properties of the mannopyranoside derivatives as antimicrobial agents. J. Taibah Univ. Sci. 18 (1). https://doi.org/10.1080/16583655.2024.2327101.

Islam, M.M., Hossain, M.A., Yamari, I., Abchir, O., Chtita, S., Ali, F., Kawsar, S.M.A., 2024. Synthesis, antimicrobial, molecular docking against bacterial and fungal proteins and in silico studies of glucopyranoside derivatives as potent antimicrobial agents. Chem. Biodivers. 2 (1), e202400932. https://doi.org/10.1002/cbdv.202400932.

Islam, S., Hosen, M.A., Ahmad, S., Qamar, M.T., Dey, S., Hasan, I., Fujii, Y., Ozeki, Y., Kawsar, S.M.A., 2022. Synthesis, antimicrobial, anticancer activities, PASS prediction, molecular docking, molecular dynamics and pharmacokinetic studies of designed methyl α-D-glucopyranoside esters. J. Mol. Struct. 1260, 132761. https://doi.org/10.1016/j.molstruc.2022.132761.

Jayavel, P., Ramasamy, V., Amaladoss, N., Renganathan, V., Shupeniuk, V.I., 2024a. A facile synthesis, characterization, DFT, ADMET and *in-silico* molecular docking analysis of novel 4-ethyl acridine-1,3,9 (2,4,10*H*)-trione. Chem. Phys. Impact 8, 100476. https://doi.org/10.1016/j.chphi.2024.100476.

Jayavel, P., Rajamanickam, R., Amaladoss, N., Ramasamy, V., Shupeniuk, V.I., 2024b. Design, one-pot novel synthesis of substituted acridine derivatives: DFT, structural characterization, ADME and anticancer DNA polymerase epsilon molecular docking studies. Mol. Phys. 122 (23), e2332493. https://doi.org/10.1080/00268976.2024.2332493.

Kabir, A.K.M.S., Kawsar, S.M.A., Bhuiyan, M.M.R., Bilkiss, B., 2008. Biological evaluation of some octanoyl derivatives of methyl 4,6-*O*-cyclohexylidene-α-D-glucopyranoside. Chittagong Univ. J. Biol. Sci. 3 (1&2), 53–64. https://doi.org/10.3329/cujbs.v3i1.13406.

Karthikeyan, S., Bharanidharan, G., Mangaiyarkarasi, R., Chinnathambi, S., Sriram, R., Gunasekaran, K., Saravanan, K., Gopikrishnan, M., Aruna, P., Ganesan, S., 2018. A cytotoxicity, optical spectroscopy and computational binding analysis of 4-[3-acetyl-5-(acetylamino)-2-methyl-2,3-dihydro-1,3,4-thiadiazole-2-yl]phenyl benzoate in calf thymus DNA. Luminescence 33 (4), 731–741. https://doi.org/10.1002/bio.3470.

Kawsar, S.M.A., Ferdous, J., 2021. Chemical synthesis of cytosine β-D-riboside esters for pathogenicity, anticancer and computational studies. J. Sci. Technol. Res. 3 (1), 23–40. https://doi.org/10.3329/jscitr.v3i1.62804.

Kawsar, S.M.A., Hosen, M.A., Chowdhury, T.S., Rana, K.M., Fujii, Y., Ozeki, Y., 2021. Thermochemical, PASS, molecular docking, drug-likeness and in silico ADMET prediction of cytidine derivatives against HIV-1 reverse transcriptase. Rev. Chim. 72 (3), 159–178. https://doi.org/10.37358/Rev.Chim.1949.

Kawsar, S.M.A., Ahmad, S., Bakri, Y.E., Laaroussi, H., Hadda, T.B., Almalki, F.A., Ozeki, Y., Goumri-Said, S., 2022a. Potential SARS-CoV-2 RdRp inhibitors of cytidine derivatives: molecular docking, molecular dynamic simulations, ADMET, and POM analyses for the identification of pharmacophore sites. PLoS One 17 (11), e0273256. https://doi.org/10.1371/journal.pone.0273256.

Kawsar, S.M.A., Kumer, A., Munia, N.S., Hosen, M.A., Chakma, U., Akash, S., 2022b. Chemical descriptors, PASS, molecular docking, molecular dynamics and ADMET predictions of glucopyranoside derivatives as inhibitors to bacteria and fungi growth. Org. Commun. Now. 15 (2), 184–203. https://doi.org/10.25135/acg.oc.122.2203.2397.

Kawsar, S.M.A., Hossain, M.A., Saha, S., Abdullah, E.M., Bhat, A.R., Ahmed, S., Jamalis, J., Ozeki, Y., 2024a. Nucleoside-based drug target with general antimicrobial screening and specific computational studies against SARS-CoV-2 main protease. ChemistrySelect 9 (15), e202304774. https://doi.org/10.1002/slct.202304774.

Kawsar, S.M.A., Munia, N.S., Saha, S., Ozeki, Y., 2024b. In silico pharmacokinetics, molecular docking and molecular dynamics simulation studies of nucleoside analogs for drug discovery-A Mini Review. Mini Rev. Med. Chem. 24 (11), 1070–1088. https://doi.org/10.2174/0113895575258033231024073521.

Kawsar, S.M.A., Islam, M., Jesmin, S., Manchur, M.A., Hasan, I., Rajia, S., 2018. Evaluation of the antimicrobial activity and cytotoxic effect of some uridine derivatives. Int. J. Biosci. 12 (6), 211–219. https://doi.org/10.12692/ijb/12.6.211-219.

Khan, R.T., Sharma, V., Khan, S.S., Rasool, S., 2024. Prevention and potential remedies for antibiotic resistance: current research and future prospects. Front. Microbiol. 15, 1455759. https://doi.org/10.3389/fmicb.2024.1455759.

Kim mi, Y., Farrah, S., Baney, R.H., 2007. Structure-antimicrobial activity relationship for silanols, a new class of disinfectants, compared with alcohols and phenols. Int. J. Antimicrob. Agents 29 (2), 217–222. https://doi.org/10.1016/j.ijantimicag.2006.08.036.

Kondapuram, S.K., Sarvagalla, S., Coumar, M.S., 2021. Docking-based virtual screening using PyRx tool: autophagy target Vps34 as a case study. Mol. Docking Comput. Drug Des. Fundam. Tech. Resour. Appl. 1 (1), 463–477. https://doi.org/10.1016/B978-0-12-822312-3.00019-9.

Koopmans, T., 1934. Über die Zuordnung von Wellenfunktionen und Eigenwerten zu den Einzelnen Elektronen Eines Atoms. Physica 1 (1–6), 104–113. https://doi.org/10.1016/S0031-8914(34)90011-2.

Krishnan, R., Binkley, J.S., Seeger, R., Pople, J.A., 1980. Self-consistent molecular orbital methods. XX A basis set for correlated wave functions. J. Chem. Phys. 72 (1), 650–654. https://doi.org/10.1063/1.438955.

Lagunin, A., Stepanchikova, A., Filimonov, D., Poroikov, V., 2000. PASS: prediction of activity spectra for biologically active substances. Bioinformatics 16 (8), 747–748. https://doi.org/10.1093/bioinformatics/16.8.747.

Lee, C., Yang, W., Parr, R.G., 1988. Development of the Colic-Salvetti correlation-energy formula into a functional of the electron density. Phys. Rev. B 37 (2), 785–789. https://doi.org/10.1103/physrevb.37.785.

Lipinski, C.A., Lombardo, F., Dominy, B.W., Feeney, P.J., 2012. Experimental and computational approaches to estimate solubility and permeability in drug discovery and development settings. Adv. Drug Deliv. Rev. 64, 4–17. https://doi.org/10.1016/j.addr.2012.09.019.

Löwenberg, B., Pabst, T., Vellenga, E., Putten, W.V., Schouten, H.C., Graux, C., Ferrant, A., Sonneveld, P., Biemond, B.J., Gratwohl, A., Greef, G.E., 2011. Cytarabine dose for acute myeloid leukemia. N. Engl. J. Med. 364 (11), 1027–1036. https://doi.org/10.1056/NEJMoa1010222.

Lu, T., Feiwu Chen, F., 2012. Multiwfn: a multifunctional wavefunction analyzer. J. Comput. Chem. 33 (5), 580–592. https://doi.org/10.1002/jcc.22885.

Lu, T., Chen, F., 2012. Quantitative analysis of molecular surface based on improved Marching Tetrahedra algorithm. J. Mol. Graph. Model. 38, 314–323. https://doi.org/10.1016/j.jmgm.2012.07.004, 2012.

Mali, S.N., Pandey, A., 2021. Molecular modeling studies on 2,4-disubstituted imidazopyridines as antimalarials: atom-based 3D-QSAR, molecular docking, virtual screening, in-silico ADMET and theoretical analysis. J. Comput. Biophys. Chem. 20 (3), 267–282. https://doi.org/10.1142/S2737416521500125.

Mali, S.N., Pandey, A., 2022. Balanced QSAR and molecular modeling to identify structural requirements of imidazopyridine analogs as anti-infective agents against trypanosomiases. J. Comput. Biophys. Chem. 21 (1), 83–114. https://doi.org/10.1142/S2737416521410015.

Maowa, J., Alam, A., Rana, K.M., Dey, S., Hosen, A., Fujii, Y., Hasan, I., Ozeki, Y., Kawsar, S.M.A., 2021. Synthesis, characterization, synergistic antimicrobial properties and molecular docking of sugar modified uridine derivatives. Ovidius Univ. Ann. Chem. 32 (1), 6–21. https://sciendo.com/issue/AUOC/32/1.

Matsumoto, R., Fujii, Y., Kawsar, S.M.A., Kanaly, R.A., Yasumitsu, H., Koide, Y., Hasan, I., Iwahara, C., Ogawa, Y., Im, C., Sugawara, S., Hosono, M., Nitta, K., Hamako, J., Matsui, T., Ozeki, Y., 2012. Cytotoxicity and glycan-binding properties of an 18 kDa lectin isolated from the marine sponge. Halichondria okadai. Toxins 4 (5), 323–338. https://doi.org/10.3390/toxins4050323.

McLean, A.D., Chandler, G.S., 1980. Contracted Gaussian basis sets for molecular calculations. I. Second-row atoms, Z=11-18. J. Chem. Phys. 72 (10), 5639–5648. https://doi.org/10.1063/1.438980.

Miehlich, B., Savin, A., Stoll, H., Preuss, H., 1989. Results obtained with the correlation energy density functionals of Becke and Lee, Yang and Parr. Chem. Phys. Lett. 157 (3), 200–206. https://doi.org/10.1016/0009-2614(89)87234-3.

Munia, N.S., Alanazi, M.M., El Bakri, Y., Alanazi, A.S., Hasan, I., Kawsar, S.M.A., Mukhrish, Y.E., 2023. Uridine derivatives: synthesis, biological evaluation, and in silico studies as antimicrobial and anticancer agents. Medicina 59 (6), 1–26. https://doi.org/10.3390/medicina59061107.

Munia, N.S., Hosen, M.A., Azzam, K.M., Al-Ghorbani, M., Baashen, M., Hossain, M.K., Ali, F., Mahmud, S., Shimu, M.S., Almalki, F.A., Hadda, T.B., 2022. Synthesis, antimicrobial, SAR, PASS, molecular docking, molecular dynamics and pharmacokinetics studies of 5′-O-uridine derivatives bearing acyl moieties: POM study and identification of the pharmacophore sites. Nucleosides Nucleotides Nucleic Acids 41 (10), 1036–1083. https://doi.org/10.1080/15257770.2022.2096898.

Murray, J.S., Politzer, P., 2011. The electrostatic potential: an overview. Wiley Interdiscip. Rev. Comput. Mol. Sci. 1 (2), 153–163. https://doi.org/10.1002/wcms.19.

Najar, A.M., Mk Omar, R., Bobtaina, E., 2020. Computational, pharmacological evaluation and comparative similarity against chloroquine for some new designed hybridized molecules and their potential use as antiviral against COVID-19 and malaria. Drug des 9 (2). https://doi.org/10.35248/2169-0138.20.9.163.

Narayanasamy, R.K., Rada, P., Zdrha, A., Ranst, M.V., Neyts, J., Tachezy, J., 2022. Cytidine nucleoside analog is an effective antiviral drug against Trichomonasvirus. J. Microbiol. Immunol. Infect. 55 (2), 191–198. https://doi.org/10.1016/j.jmii.2021.08.008.

Nepolraj, A., Shupeniuk, V.I., Sathiyaseelan, M., Prakash, N., 2021. Synthesis of new 3-(hydroxymethyl)-2-phenyl-2, 3 dihydroquinolinone and in-silico evaluation of COVID-19 main protease inhibitor. Vietnam J. Chem. 59 (4), 511–521. https://doi.org/10.1002/vjch.202000221.

Pal, R., Chattaraj, P.K., 2021. Chemical reactivity from a conceptual density functional theory perspective. J. Indian Chem. Soc. 98 (1), 100008. https://doi.org/10.1016/j.jics.2021.100008.

Pires, D.E., Blundell, T.L., Ascher, D.B., 2015. pkCSM: predicting small-molecule pharmacokinetic and toxicity properties using graph-based signatures. J. Med. Chem. 58 (9), 4066–4072. https://doi.org/10.1021/acs.jmedchem.5b00104.

Pourkarim, F., Pourtaghi-Anvarian, S., Rezaee, H., 2022. Molnupiravir: a new candidate for COVID-19 treatment. Pharmacol. Res. Perspect. 10 (1), 1–7. https://doi.org/10.1002/prp2.909.

Rana, K.M., Ferdous, J., Hosen, A., Kawsar, S.M.A., 2020. Ribose moieties acylation and characterization of some cytidine analogs. J. Sib. Fed. Univ. Chem. 13 (4), 465–478. https://elib.sfu-kras.ru/handle/2311/137871.

Rana, K.M., Maowa, J., Alam, A., Dey, S., Hosen, A., Hasan, I., Fujii, Y., Ozeki, Y., Kawsar, S.M.A., 2021. In silico DFT study, molecular docking, and ADMET predictions of cytidine analogs with antimicrobial and anticancer properties. Silico Pharmacol 9 (1). https://doi.org/10.1007/s40203-021-00102-0.

Retailleau, P., Colloc'h, N., Vivarès, D., Bonneté, F., Castro, B., El Hajji, M., Mornon, J.P., Monard, G., Prangé, T., 2004. Complexed and ligand-free high-resolution structures of urate oxidase (Uox) from *Aspergillus flavus*: a reassignment of the active-site binding mode. Acta Crystallogr. 60 (3), 453–462. https://doi.org/10.1107/S0907444903029718.

Rohloff, J.C., Fowler, C., Ream, B., Carter, J.D., Wardle, G., Fitzwater, T., 2015. Practical synthesis of cytidine-5-carboxamide-modified nucleotide reagents. Nucleosides Nucleotides Nucleic Acids 34 (3), 180–198. https://doi.org/10.1080/15257770.2014.978011.

Roy, D.R., Parthasarathi, R., Maiti, B., Subramanian, V., Chattaraj, P.K., 2005. Electrophilicity as a possible descriptor for toxicity prediction. Bioorg. Med. Chem. 13 (10), 3405–3412. https://doi.org/10.1016/j.bmc.2005.03.011.

Salam, M.A., Al-Amin, M.Y., Salam, M.T., Pawar, J.S., Akhter, N., Rabaaan, A.A., Alqumber, M.A.A., 2023. Antimicrobial resistance: a growing serious threat for global public health. Healthcare (Basel) 11 (13), 1946. https://doi.org/10.3390/healthcare11131946.

Sampathkumar, J., Dalavi, P.A., Venkatesan, J., Amaladoss, N., Rajamanickam, R., 2024. Synthesis, spectroscopic, SC-XRD, DFT, RAHBs, RDG, molecular docking and *in vitro* anticancer evaluation of ethyl 1,2,5,6-tetrahydro-4-hydroxy-2,6-diphenylpyridine-3-carboxylate. J. Mol. Struct. 1305, 137731. https://doi.org/10.1016/j.molstruc.2024.137731.

Shamsuddin, T., Hosen, M.A., Alam, M.S., Emran, T.B., Kawsar, S.M.A., 2021. Uridine derivatives: antifungal, PASS outcomes, ADMET, drug-likeliness, molecular docking, and binding energy calculations. Med. Sci. Int. Med. J. 10 (4), 1373–1386. https://doi.org/10.5455/medscience.2021.05.175.

Sharma, V., Chitranshi, N., Agarwal, A.K., 2014. Significance and biological importance of pyrimidine in the microbial world. Int. J. Med. Chem. 2014 (1), 202784. https://doi.org/10.1155/2014/202784.

Stephens, P.J., Devlin, F.J., Chabalowski, C.F., Frisch, M.J., 1994. Ab Initio calculation of vibrational absorption and circular dichroism spectra using density functional force fields. J. Phys. Chem. 98 (5), 11623–11627. https://doi.org/10.1021/j100096a001.

Stresemann, C., Lyko, F., 2008. Modes of action of the DNA methyltransferase inhibitors azacytidine and decitabine. Int. J. Cancer 123 (1), 8–13. https://doi.org/10.1002/ijc.23607.

Sultana, S., Hossain, M.A., Biswas, S., Saleh, M.A., Ali, F., Kawsar, S.M.A., 2024. Chemical reactivity, molecular electrostatic potential, FTIR, NMR, in vitro, and in silico studies of mannopyranoside derivatives : 3-Nitrobenzoylation leads to improve antimicrobial activity. Chem. Phys. Impact 9, 100692. https://doi.org/10.1016/j.chphi.2024.100692.

Suresh, C.H., Remya, G.S., Anjalikrishna, P.K., 2022. Molecular electrostatic potential analysis: a powerful tool to interpret and predict chemical reactivity. Wiley Interdiscip. Rev. Comput. Mol. Sci. 12 (5). https://doi.org/10.1002/wcms.1601.

Tabassum, R., Kawsar, S.M.A., Alam, A., Saha, S., Hosen, A., Hasan, I., Prinsa, M., Chalkha, M., 2024. Synthesis, spectral characterization, biological, FMO, MEP, molecular docking, and molecular dynamics simulation studies of cytidine derivatives as antimicrobial and anticancer agents. Chem. Phys. Impact 9, 100724. https://doi.org/10.1016/j.chphi.2024.100724.

Tiralongo, J., Moran, A.P., 2010. Bacterial lectin-like interactions in cell recognition and adhesion. Microb. Glycobiol. 1 (2), 549–565. https://doi.org/10.1016/B978-0-12-374546-0.00027-4.

Toschi, L., Finocchiaro, G., Bartolini, S., Gioia, V., Cappuzzo, F., 2015. Role of gemcitabine in cancer therapy. Future Oncol. 1 (1), 7–17. https://doi.org/10.1517/14796694.1.1.7.

Vogler, W., Miller, D., Keller, J., 1976. 5-Azacytidine (NSC 102816): a new drug for the treatment of myeloblastic leukemia. Blood 48 (3), 331–337. https://doi.org/10.1182/blood.V48.3.331.331.

Wang, P., Cheng, T., Pan, J., 2023. Nucleoside analogs: a review of its source and separation processes. Molecules 28 (20), 7043. https://doi.org/10.3390/molecules28207043.

Zhao, M., Ma, J., Li, M., Zhan, Y., Jiang, B., Zhao, X., Huai, C., Shen, L., Zhang, N., He, L., Qin, S., 2021. Cytochrome p450 enzymes and drug metabolism in humans. Int. J. Mol. Sci. 22 (23), 1–16. https://doi.org/10.3390/ijms222312808.